

The escape fraction from galactic labyrinths of ionizing photons produced by high-z AGNs



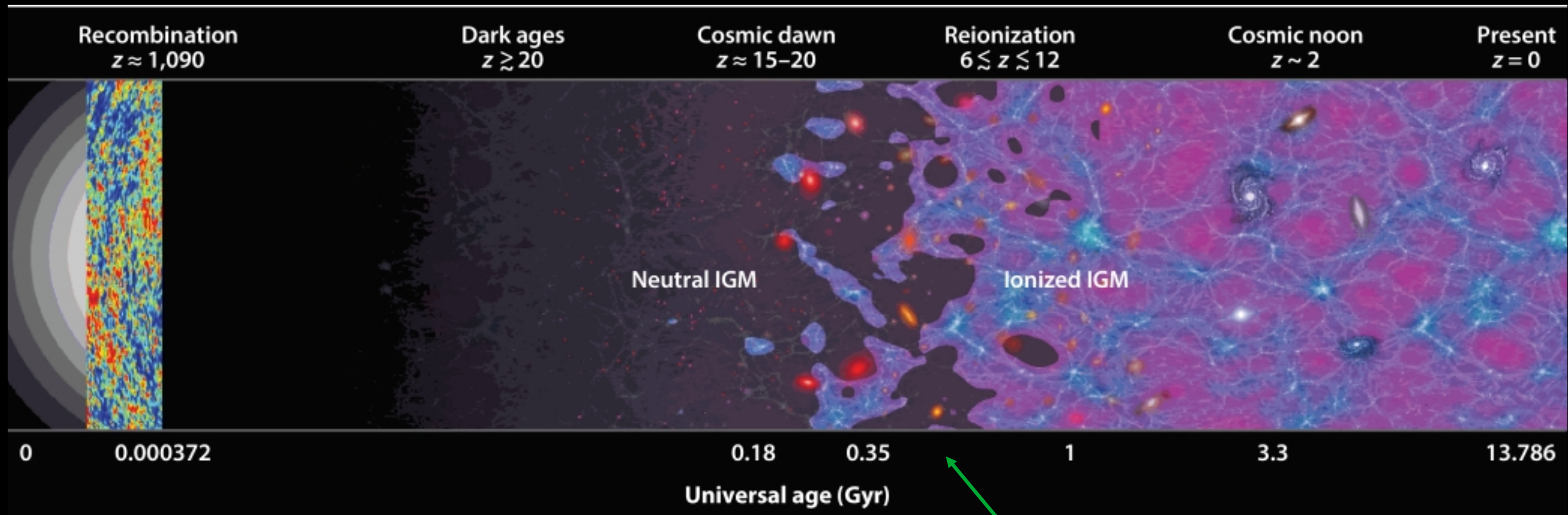
Andrea Grazian (INAF-OAPd)

Escape of Lyman radiation from galactic labyrinths

OAC, Kolymbari, Crete - April 7-11, 2025

Reionization: What ?

Hydrogen Reionization: major phase transition of the Universe



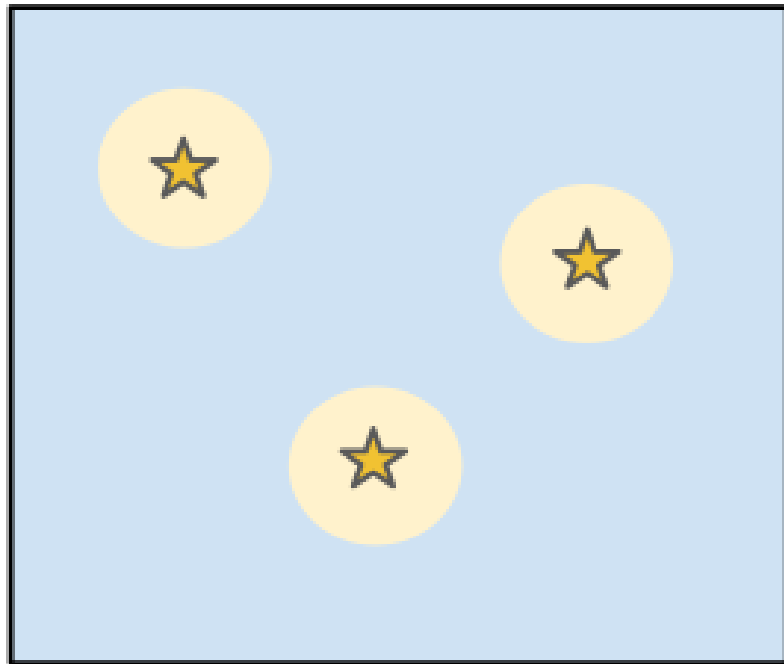
Robertson 2022

Chakraborty & Choudhury 2025

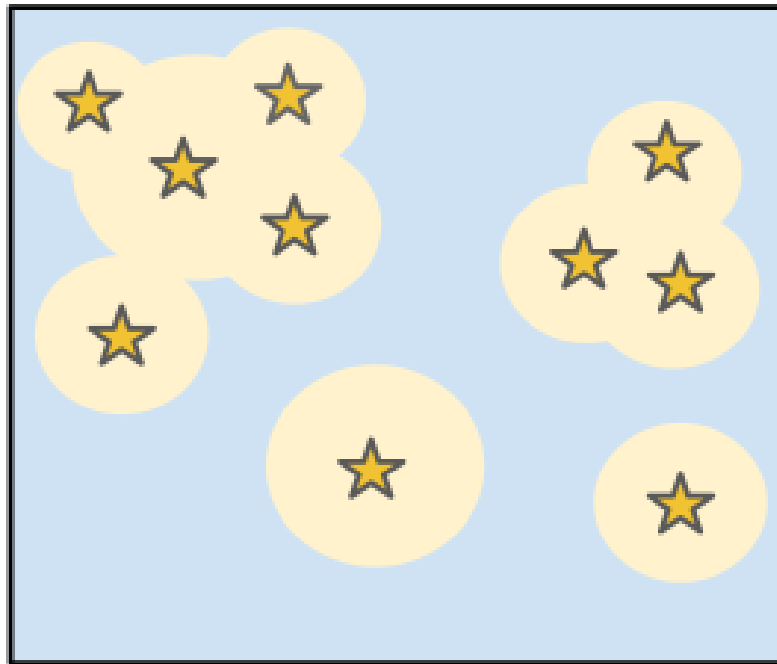
Hydrogen reionization
End of Dark Ages

Reionization: How ?

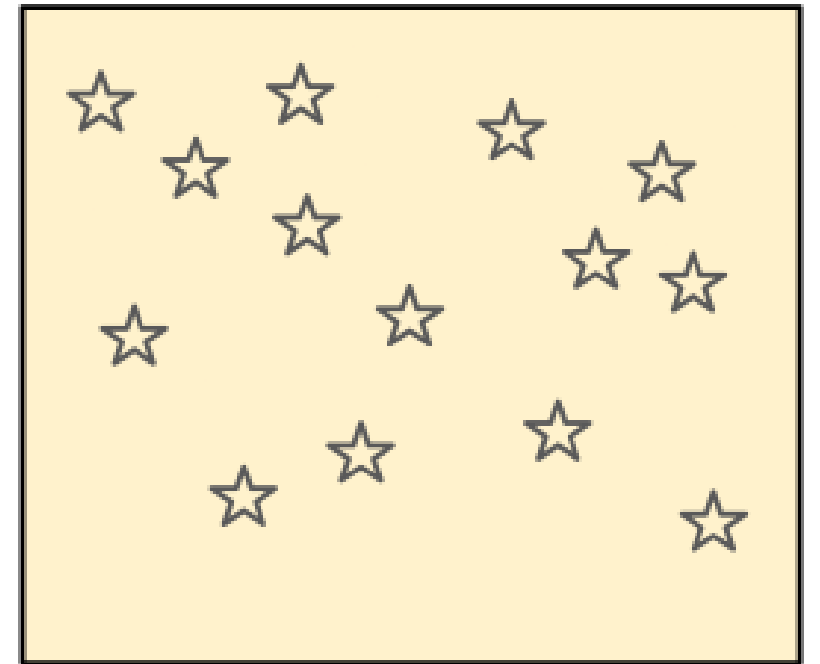
Pre Overlap



Overlap



Post Overlap



Chakraborty & Choudhury 2025

Overlap of ionizing bubbles
around first sources of light.

Epoch of Reionization: When ?

Gunn-Peterson troughs suggest
reionization ending at $z=5.2-5.5$

Ultra Late Reionization

(Fan et al. 2006; Keating et al.
2020; Becker et al. 2021; Bosman
et al. 2021; Zhu et al. 2022;
Gaikwad et al. 2023)

Gunn-Peterson effect

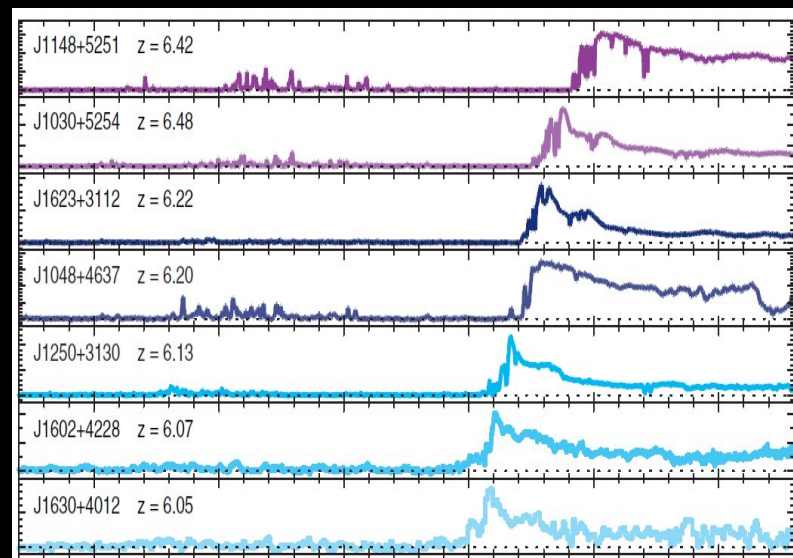
Planck 2020 result: $\tau=0.0506\pm0.0086$

$z_{\text{reion}}\sim 7.0$ $\Delta z < 1.1-2.8$

Rapid process

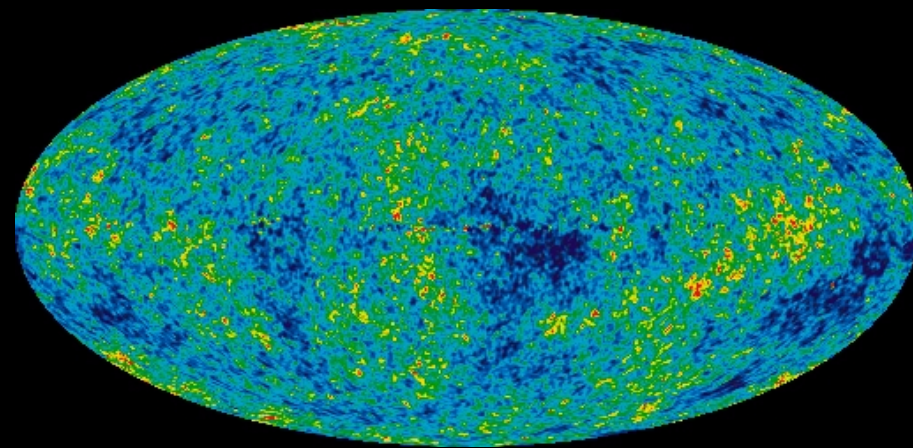
(Akrami et al. 2020; Reichardt et al. 2021)

Thomson scattering optical
depth measured in CMB



$z_{\text{reion}} > 5.2$

+



$z_{\text{reion}} < 8.0$

$\Rightarrow 5.2 < z < 8.0$

Fast and Ultra-Late Reionization

Sources of Reionization

What are the sources of first light ?

Can they sustain reionization ?

Two main suspects: Galaxies and AGNs

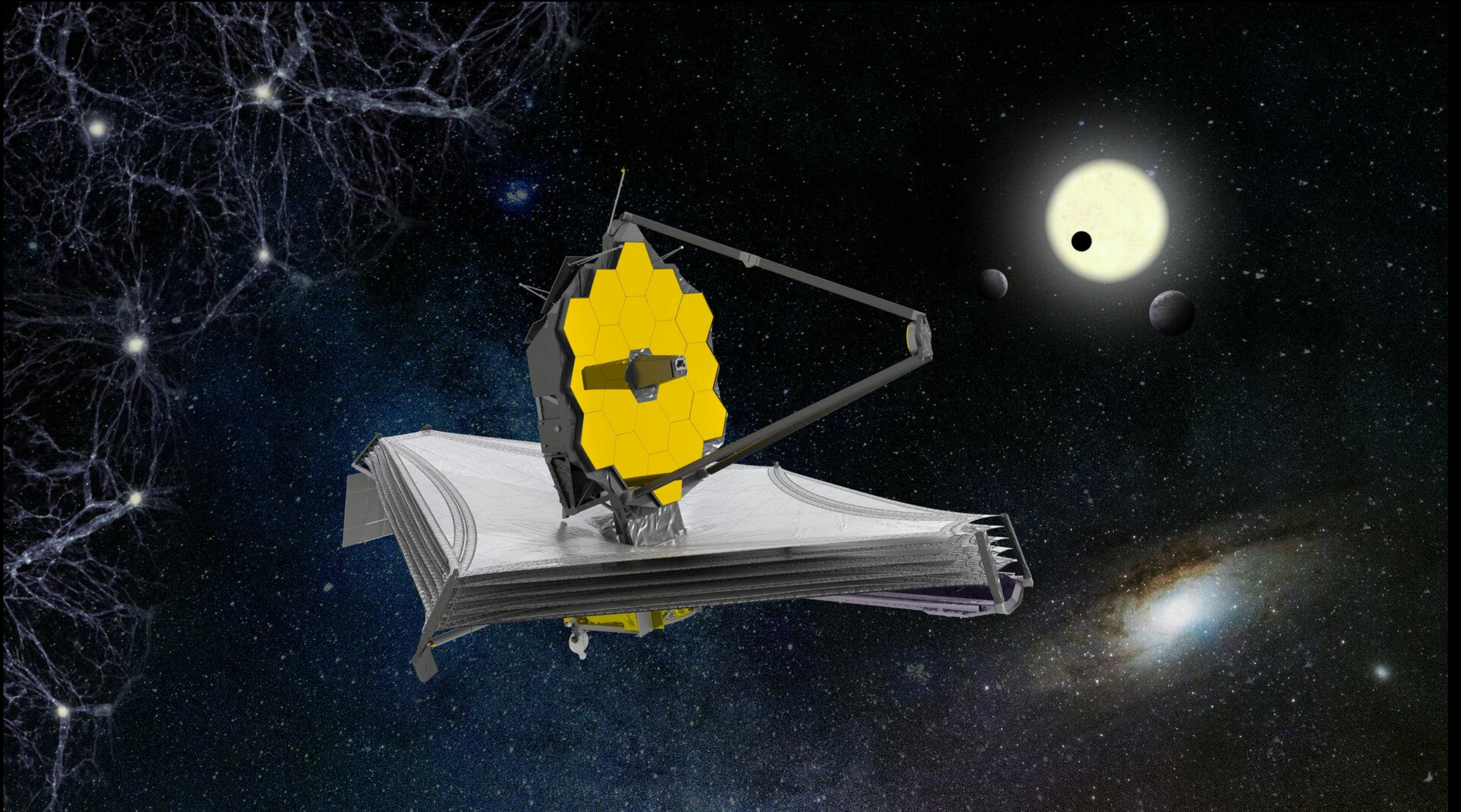


Galaxies

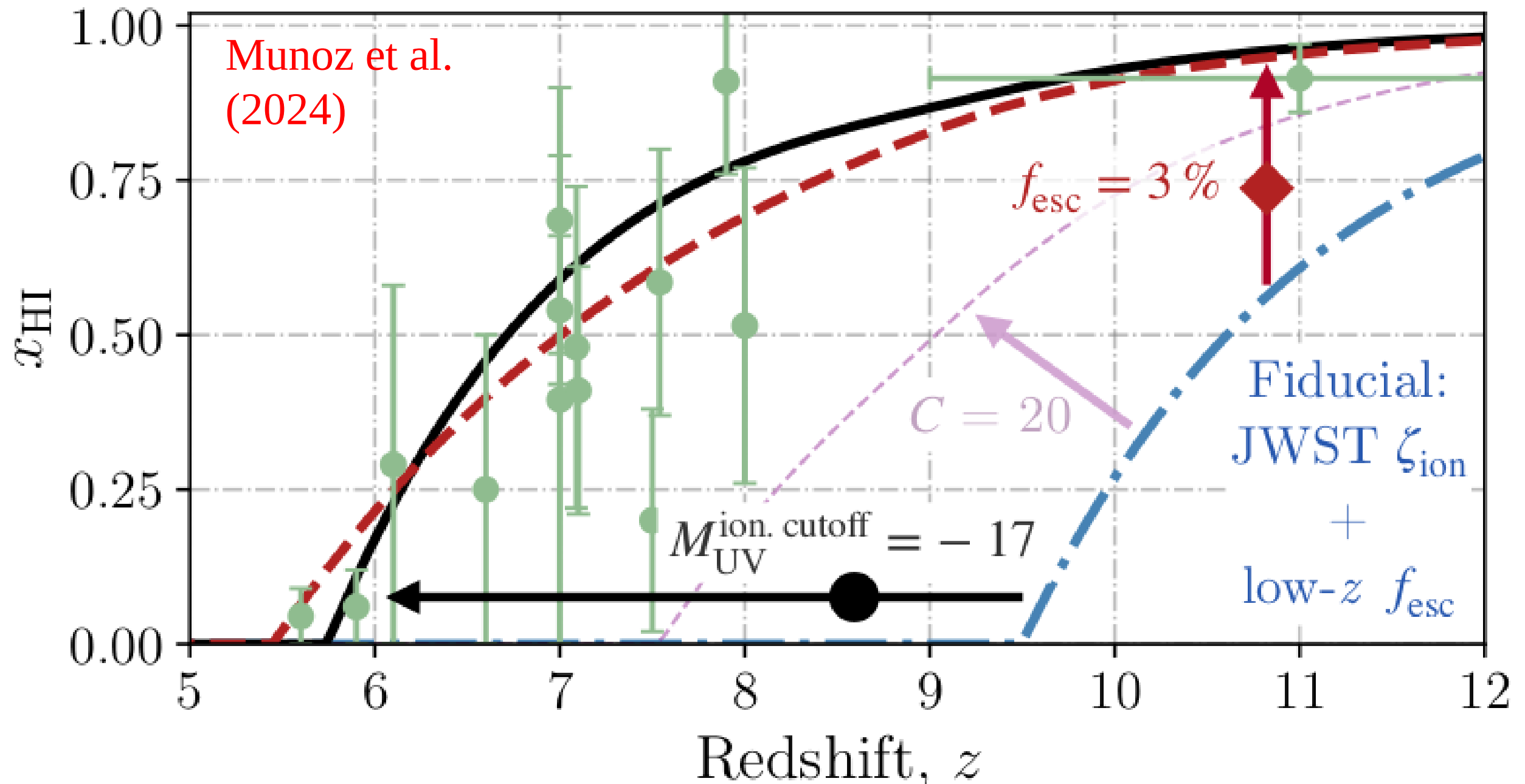


AGN

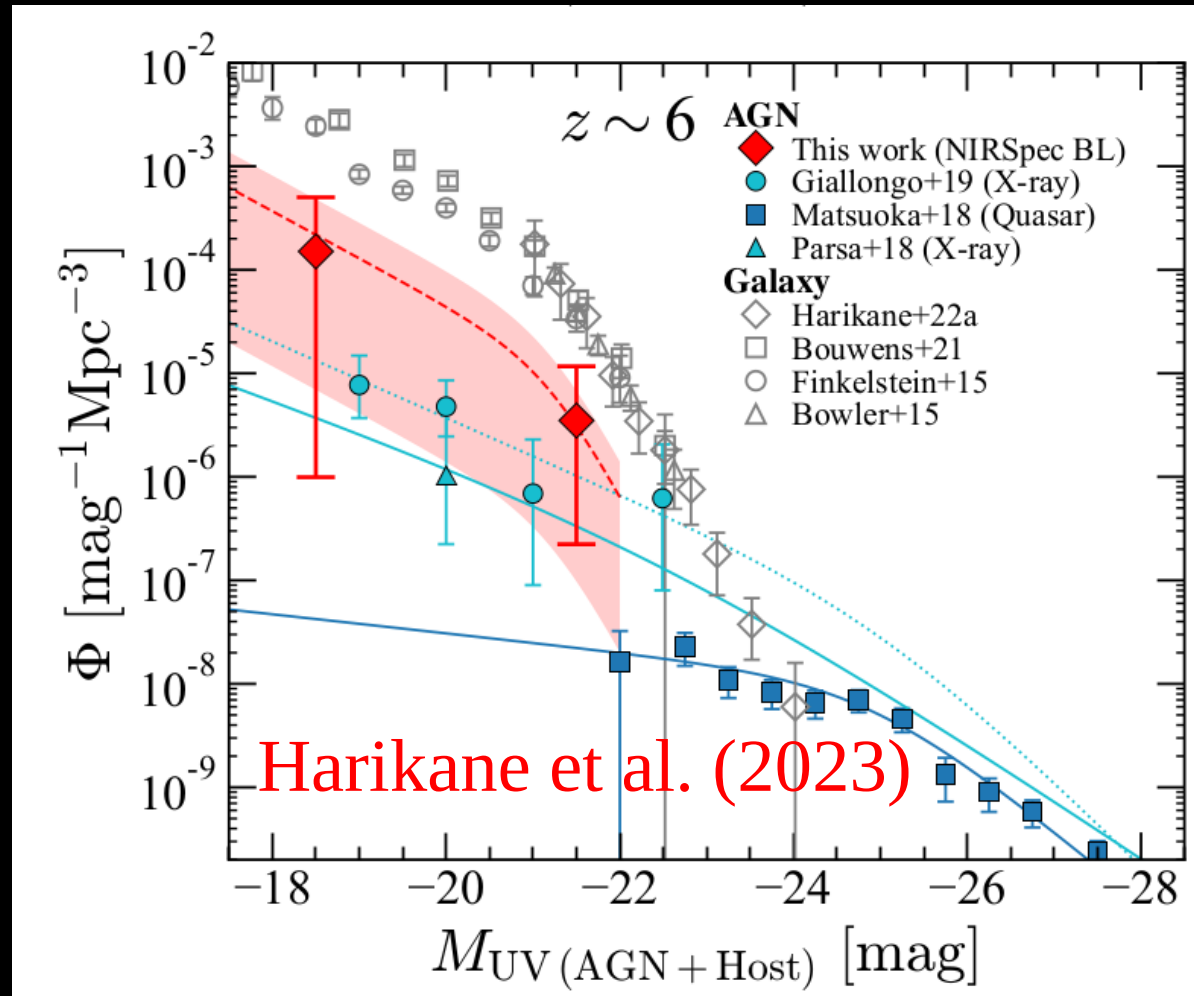
The revolution of JWST...



Faint Star Forming Galaxies: too fast reionization process.
Bright and rare sources are required to match current data.



JWST has revealed an emergent population of faint AGNs at $4 < z < 11$



Kocevski et al. 2023, 2024; Harikane et al. 2023; Fujimoto et al. 2023; Matthee et al. 2024; Maiolino et al. 2024; Greene et al. 2024; Furtack et al. 2024; and many others...

Type-1 AGNs at $z \sim 6$ produce 60% of ionizing radiation (assuming $f_{\text{esc}} \sim 50\%$).

Type-2 AGNs (Scholtz et al. 2024) are 2 times the Type-1 AGNs.

Production of ionizing radiation

$$\dot{N}_{ion}(z) = \int_{\nu_H}^{\nu_{up}} \frac{\rho_\nu}{h_p \nu} d\nu$$

Ionization rate

$$\rho_\nu = \int_{L_{min}}^{\infty} f_{esc}(L, z) \Phi(L, z) L_\nu(L) dL ,$$

Ionizing
Luminosity
Density

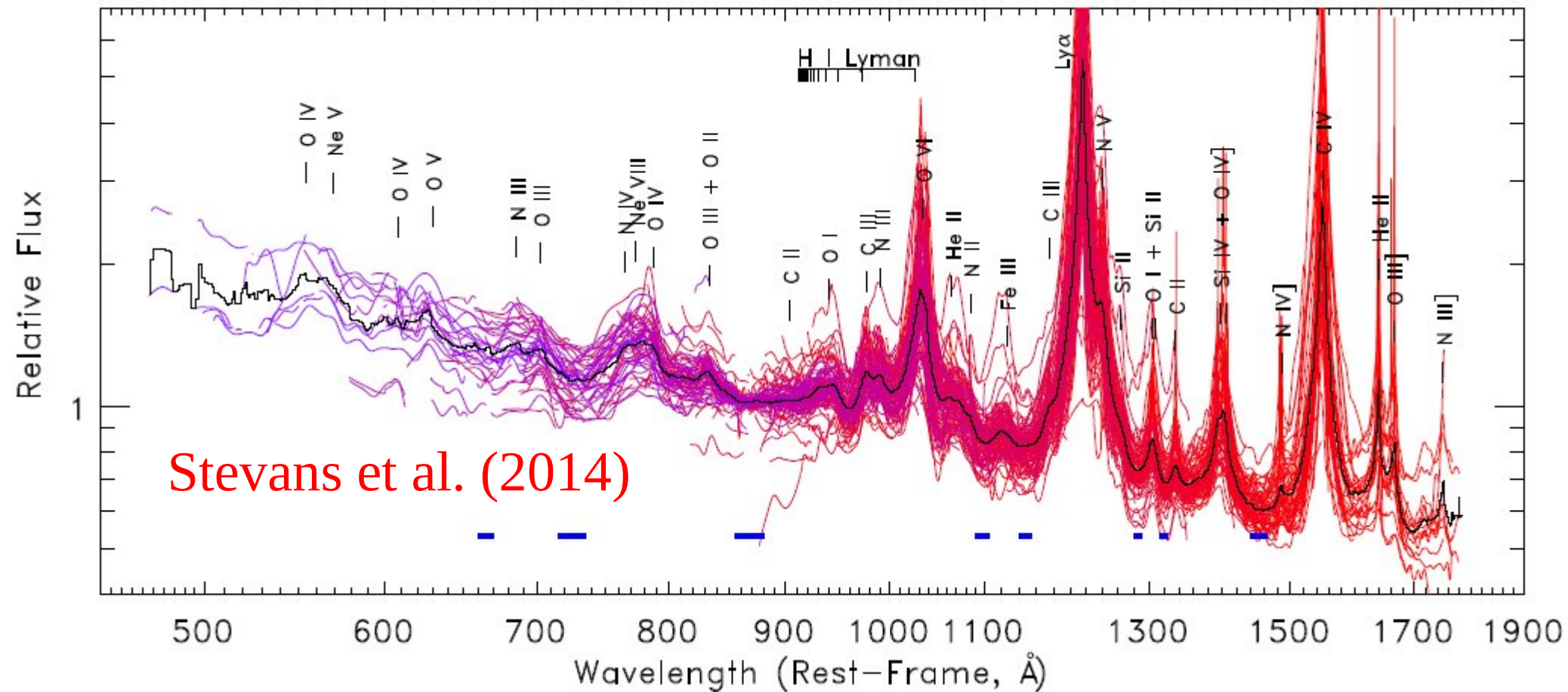
Luminosity Function at
1450Å rest frame

Spectral Energy Distribution
(L1450/L900 ratio)

f_{esc}

Escape fraction of LyC photons
Most critical parameter

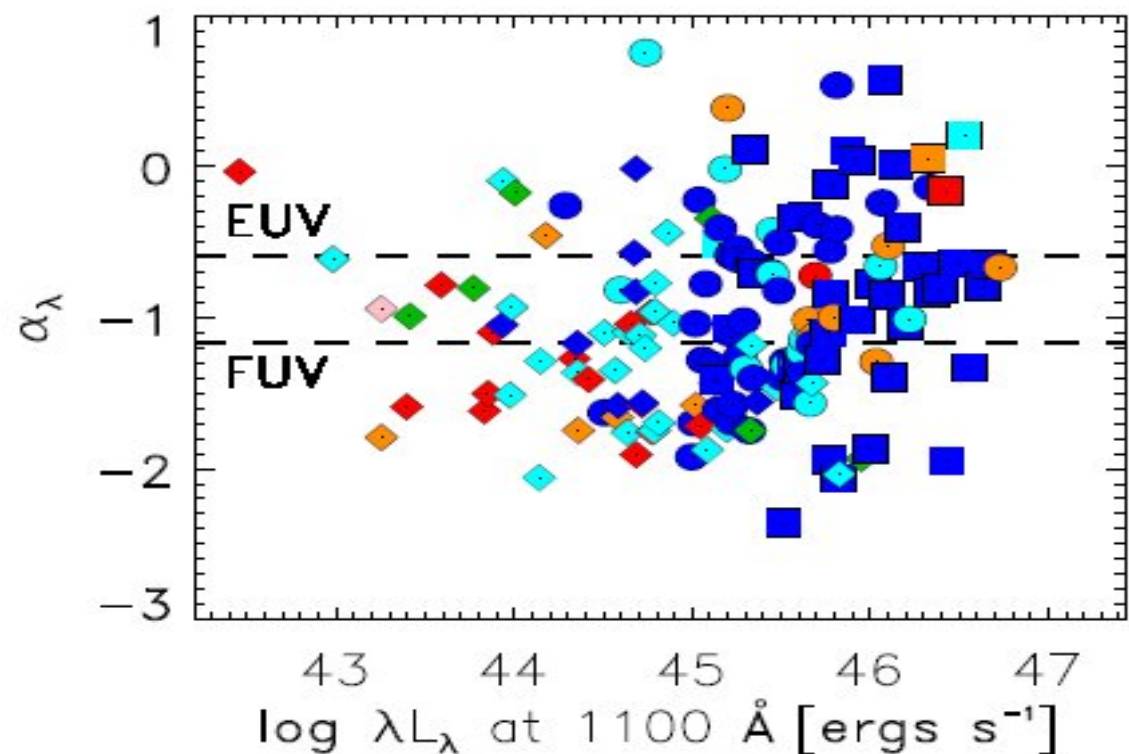
AGN LyC fesc from spectra



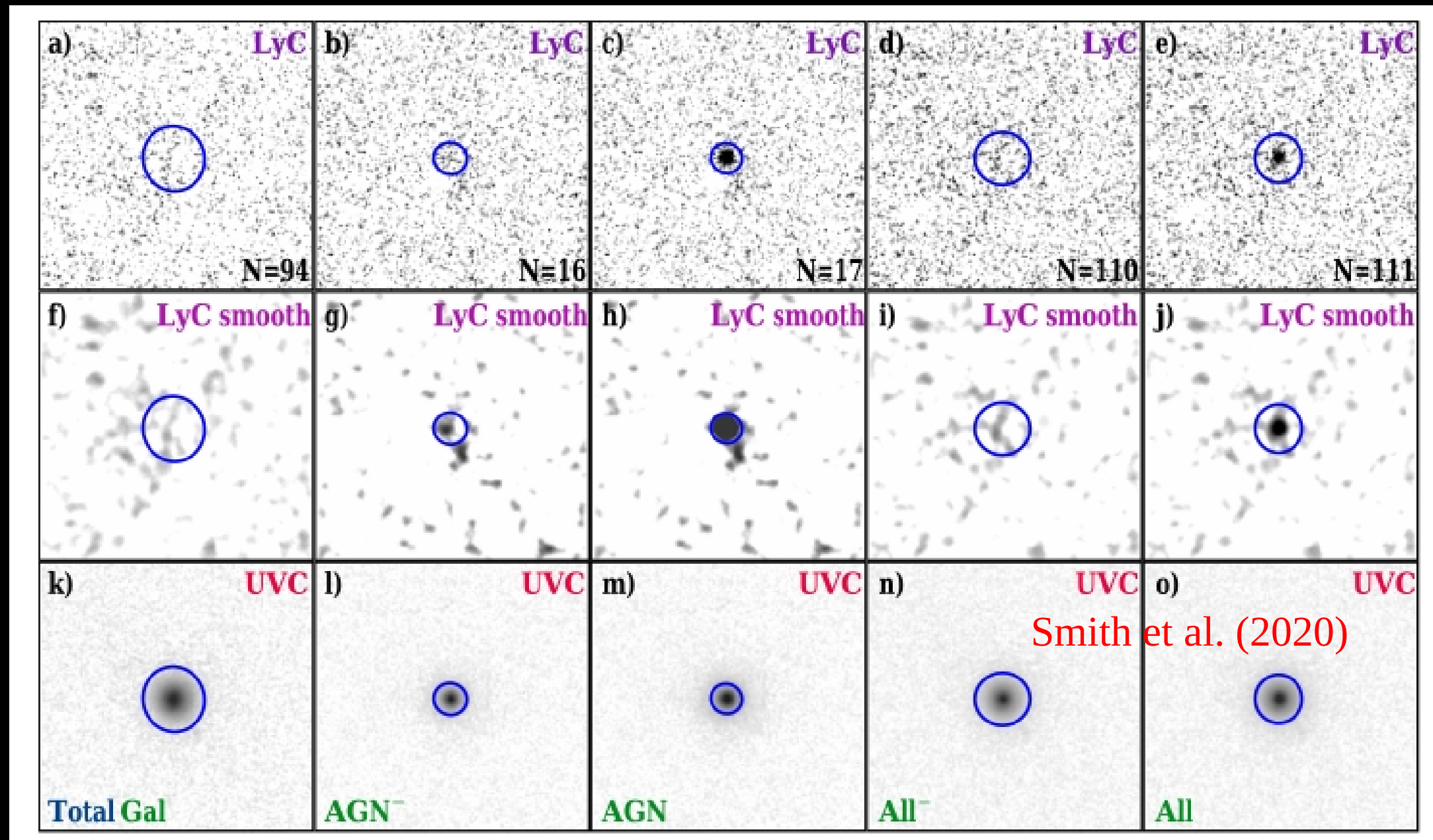
Stevans et al. (2014) find significant LyC emission in 159 low-luminosity AGNs at $z < 1.5$

(both type 1 and type 1.8-1.9 AGNs)

Escape fraction of AGNs is $\sim 100\%$ at low- z

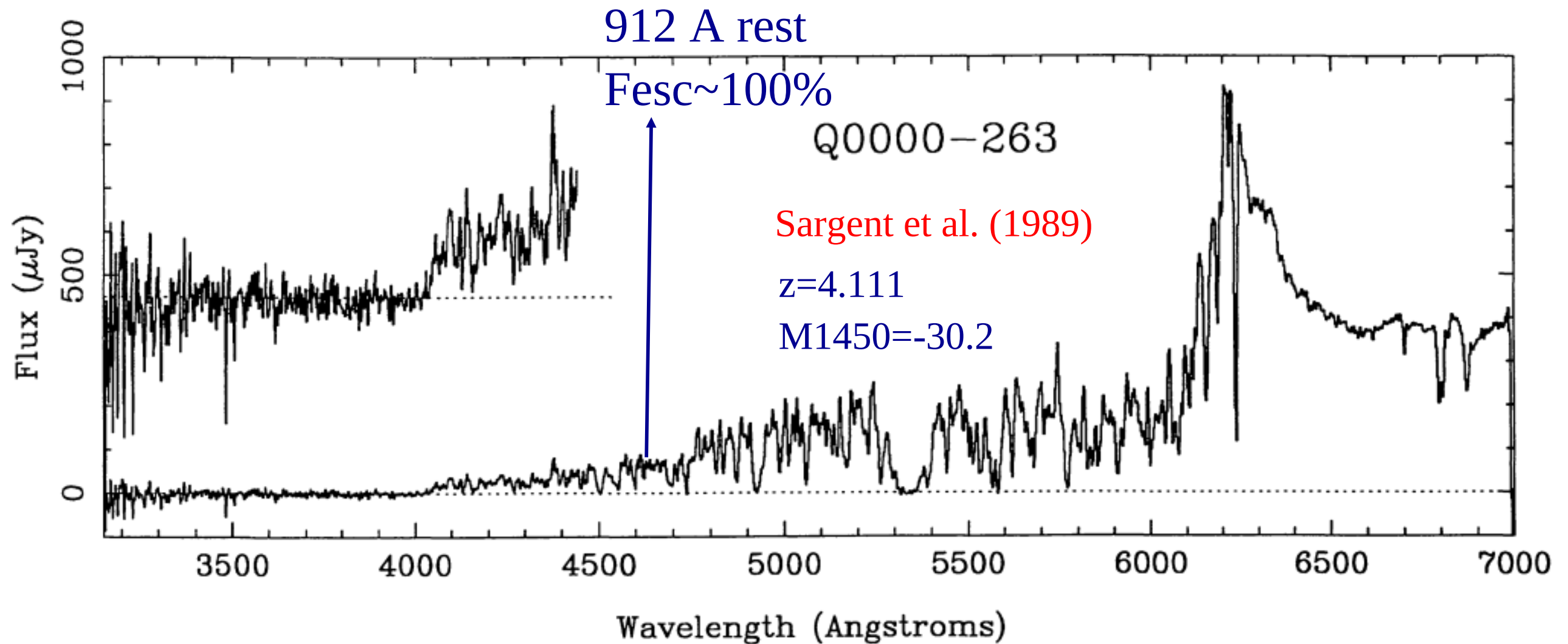


LyC fesc of $z \sim 3$ AGN



The stack of 17 AGN dominates the LyC production from $z \sim 2.3$ – 4.3 by a factor of ~ 10 compared to all 94 galaxies without AGN.

Very bright QSOs show high fesc

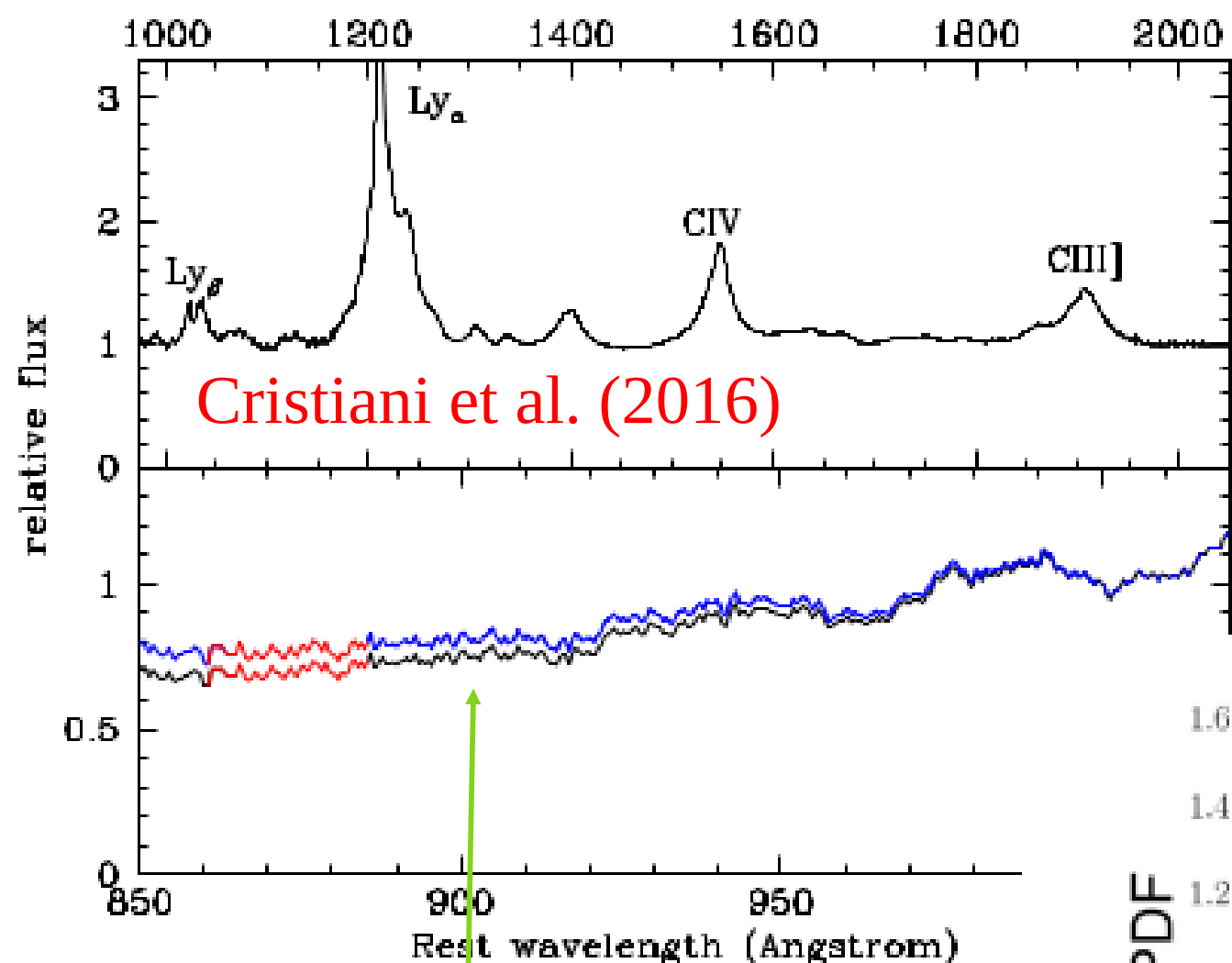


4 bright QSOs at $z \sim 4$ from Sargent et al. (1989) show high LyC fesc

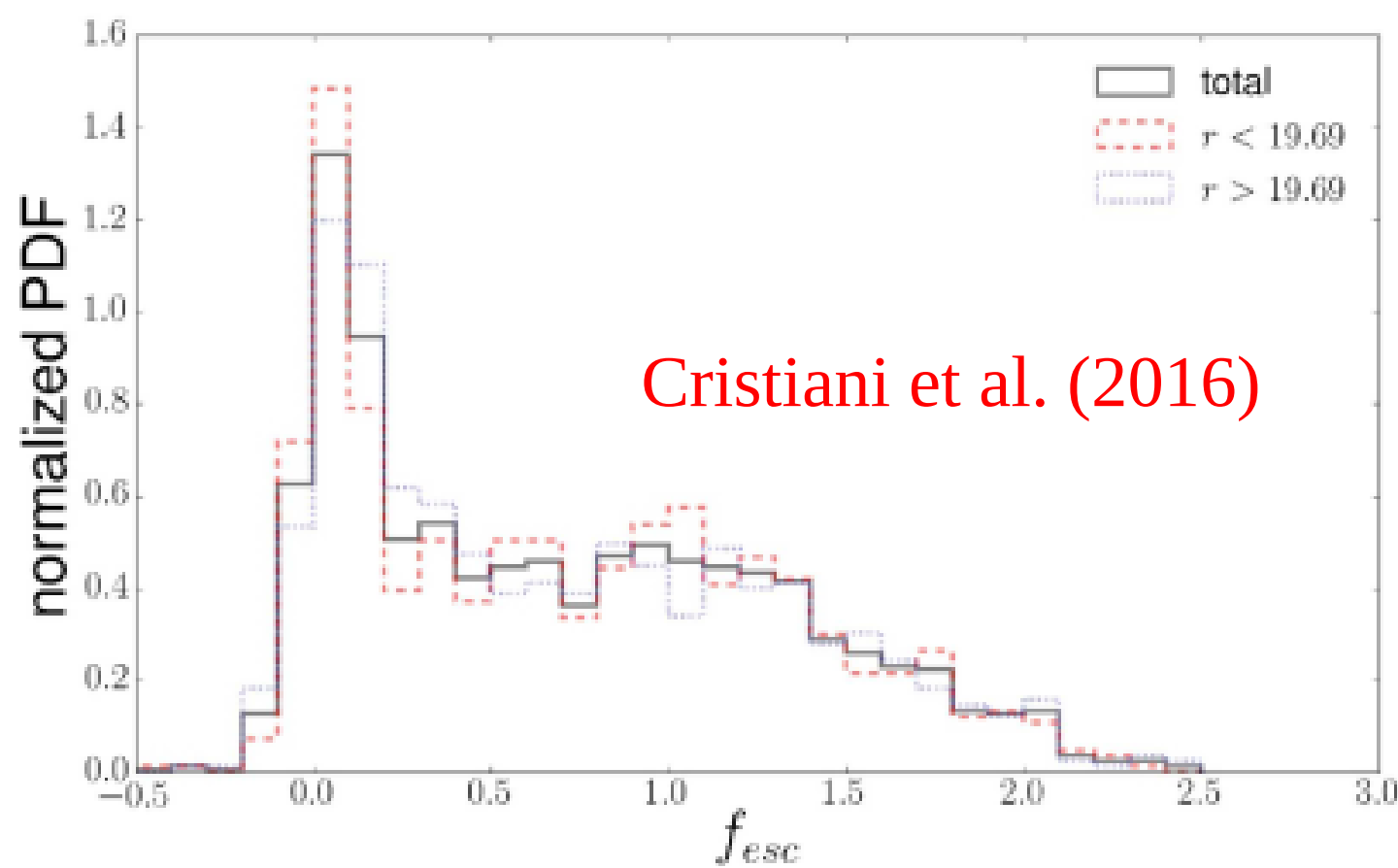
The LyC Escape Fraction of bright QSOs

~1600 QSOs at $3.6 < z < 4.0$
and $M_{1450} < -26$

($L \sim 5L^*$) have average LyC
 $f_{\text{esc}} \sim 75\%$ (or more). See
also Romano et al. (2019)



No break at
912 Å rest frame
Large LyC f_{esc}



LyC emission of high- z QSOs

Bright high- z QSOs are strong LyC emitters

Direct detection of LyC up to $z=5.5$

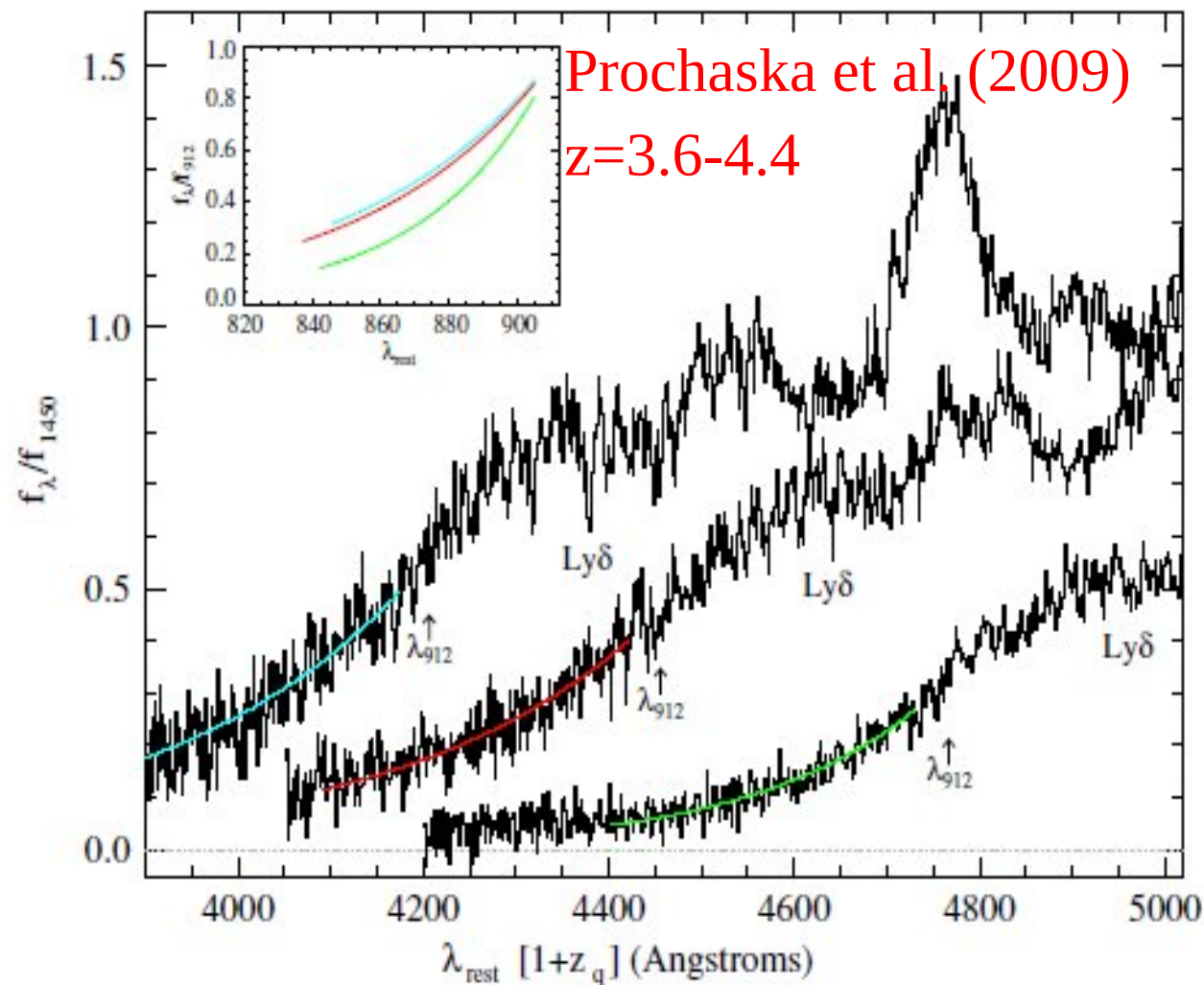


Figure 2. Stacked spectrum for three of our redshift bins (cyan: $z = [3.59, 3.63]$; red: $z = [3.86, 3.92]$; green: $z = [4.13, 4.34]$) plotted against rest-frame wavelengths redshifted to the mean quasar redshift for the bin. Overplotted on each spectrum is our best-fit model for the absorbed flux below λ_{912} due to the Lyman limit opacity. These same curves are shown in the sub-panel against rest wavelengths. The emission lines are from Lyman series and metal-line transitions.

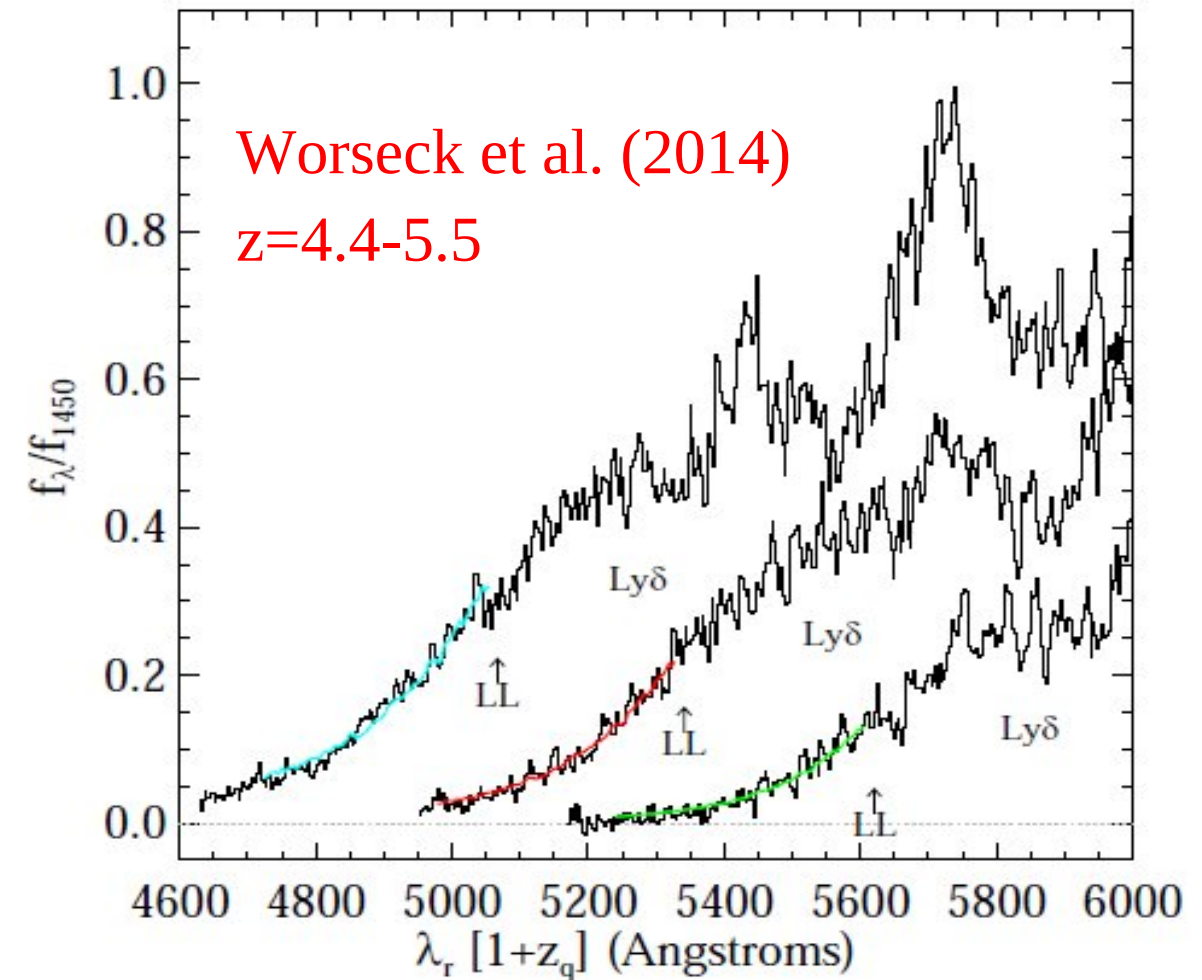
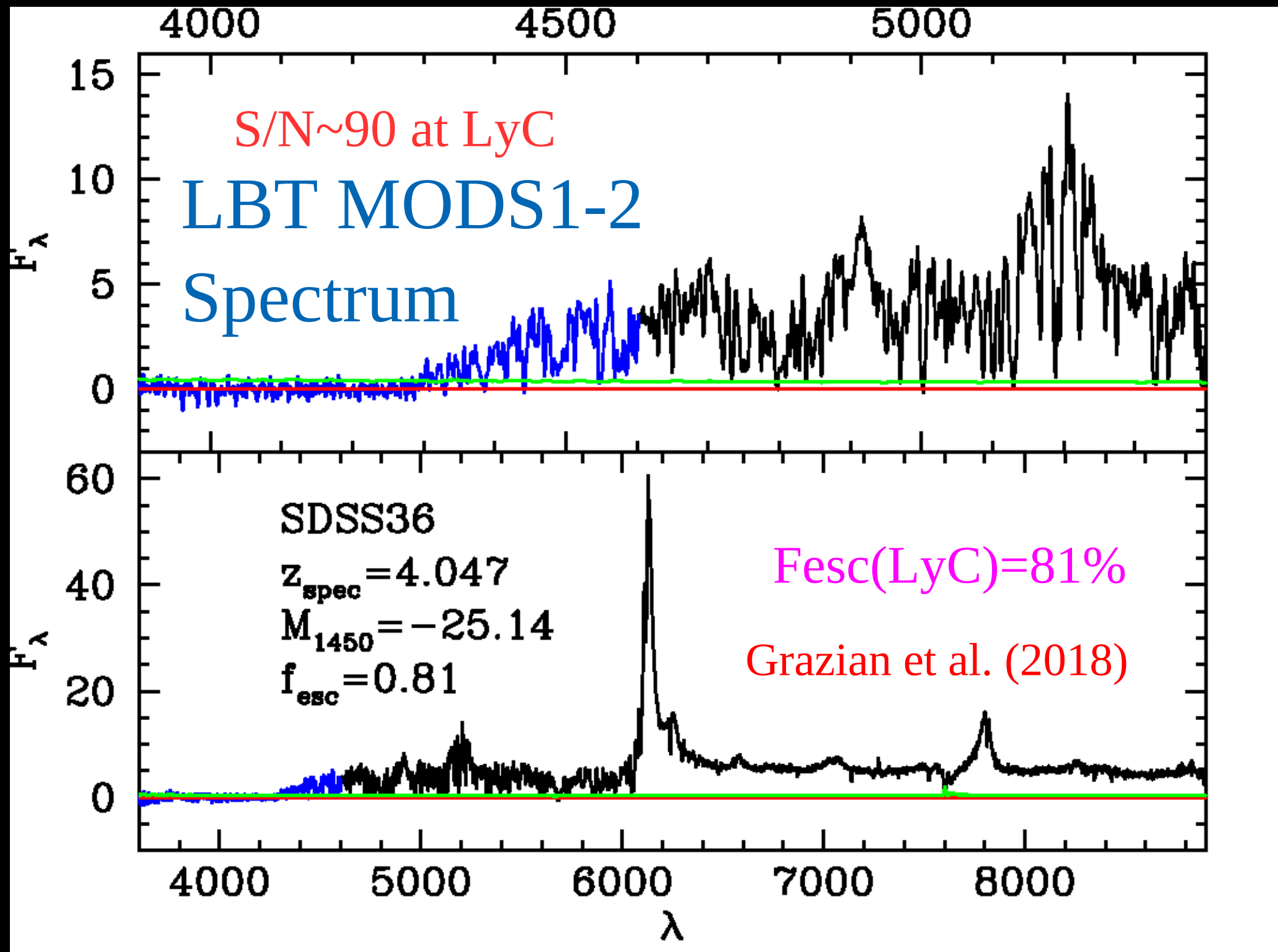


Figure 6. Stacked normalized rest-frame quasar spectra from the GGG survey generated for three redshift intervals: $z_{\text{em}} = [4.4, 4.7]$, $[4.7, 5.0]$, and $[5.0, 5.5]$. These spectra are plotted in a pseudo-observer frame defined as $\lambda_r (1 + z_q)$ with, z_q the average redshift of the quasars in each interval. The Ly δ emission (strongly affected by IGM absorption for the two high- z bins) and the onset of the Lyman limit are marked for each stacked spectrum. Ly β and Ly γ emission lines of the background quasars are clearly visible. Overplotted on these stacked spectra are the best-fitting models which provide measurements for the mean free path $\lambda_{\text{mfp}}^{912}$.

The LyC Escape Fraction of faint AGNs

f_{esc}

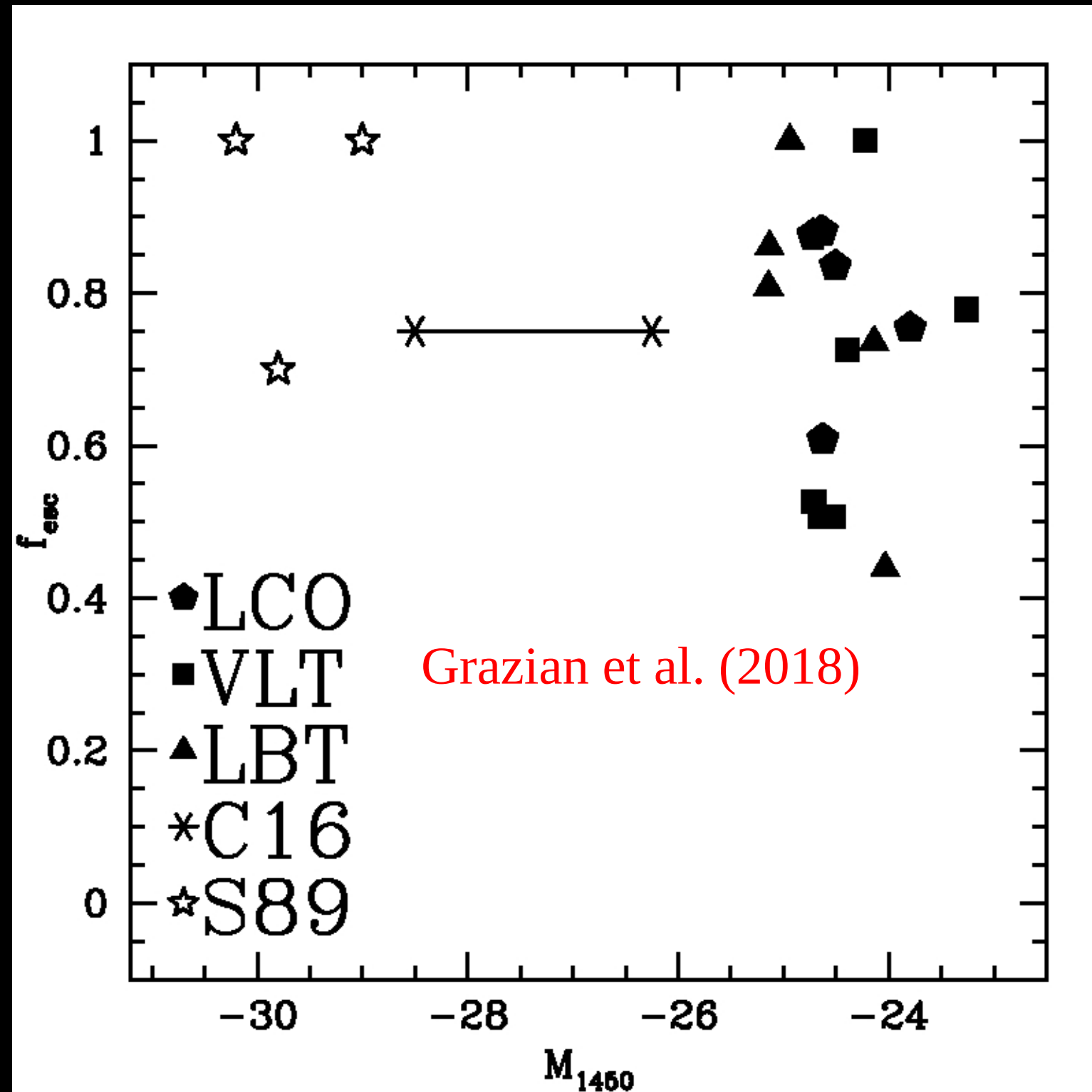
Data reduced by Spectroscopic center in Milano



Name	z_{spec}^{new}	$f_{esc}(LyC)$	S/N	M_{1450}
SDSS36	4.047	0.81	87	-25.14
SDSS32	3.964	0.86	33	-25.13
COSMOS775	3.609	0.74	31	-24.14
SDSS37	4.173	1.00	121	-24.94
NDWFSJ05	3.900	0.44	12	-24.03
SDSS04	3.768	0.73	96	-24.39
COSMOS1782	3.748	0.78	72	-23.26
SDSS20	3.899	0.53	58	-24.71
SDSS27	3.604	1.00	42	-24.22
COSMOS955	3.715	0.51	84	-24.65
COSMOS1311	3.736	0.51	29	-24.53
SDSS3777	3.723	0.61	26	-24.62
SDSS3793	3.743	0.84	12	-24.51
SDSS3785	3.769	0.88	20	-24.63
SDSS3832	3.663	0.88	11	-24.72
UDS10275	4.096	0.75	27	-23.80
MEAN	3.82	0.74		-24.46

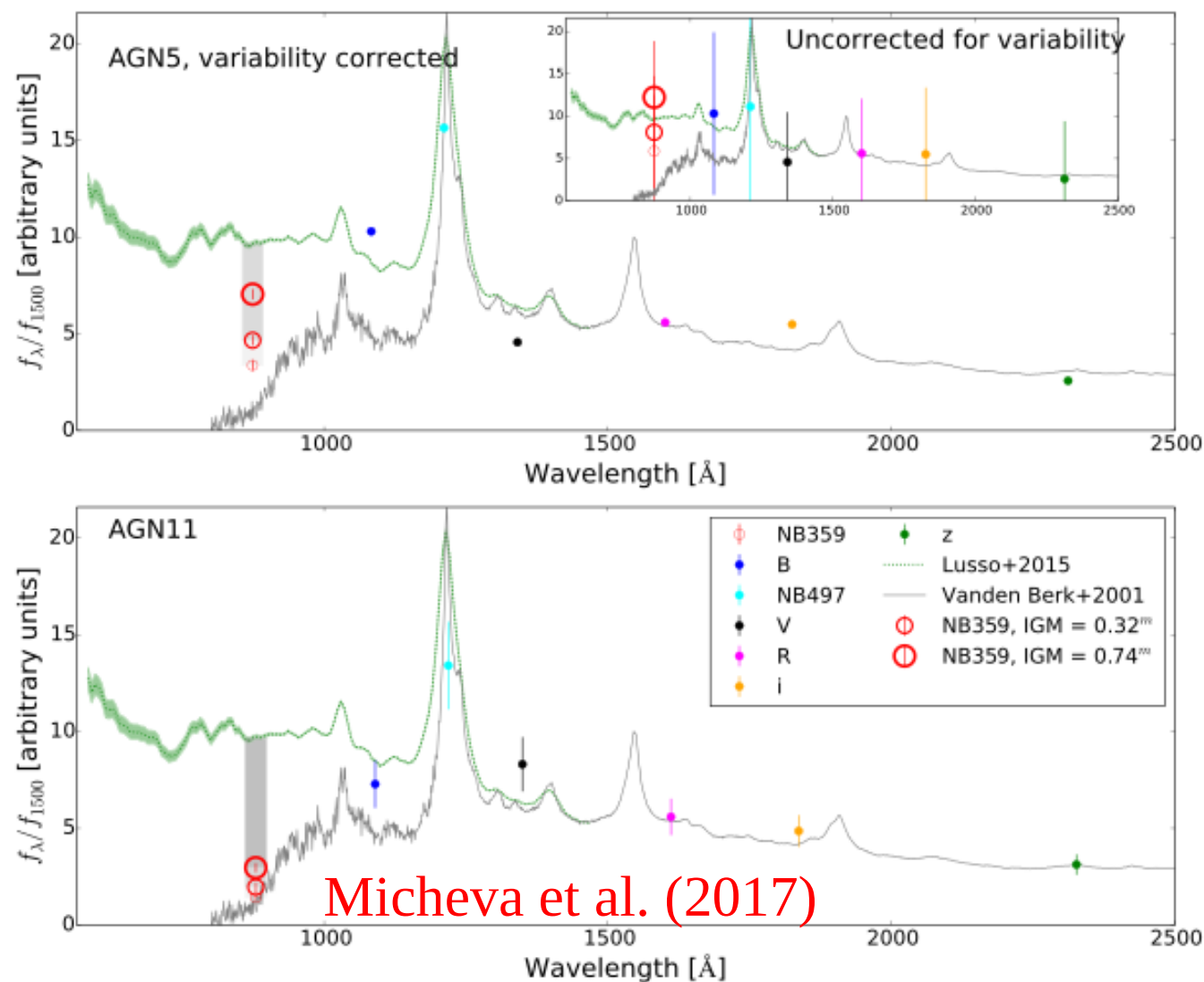
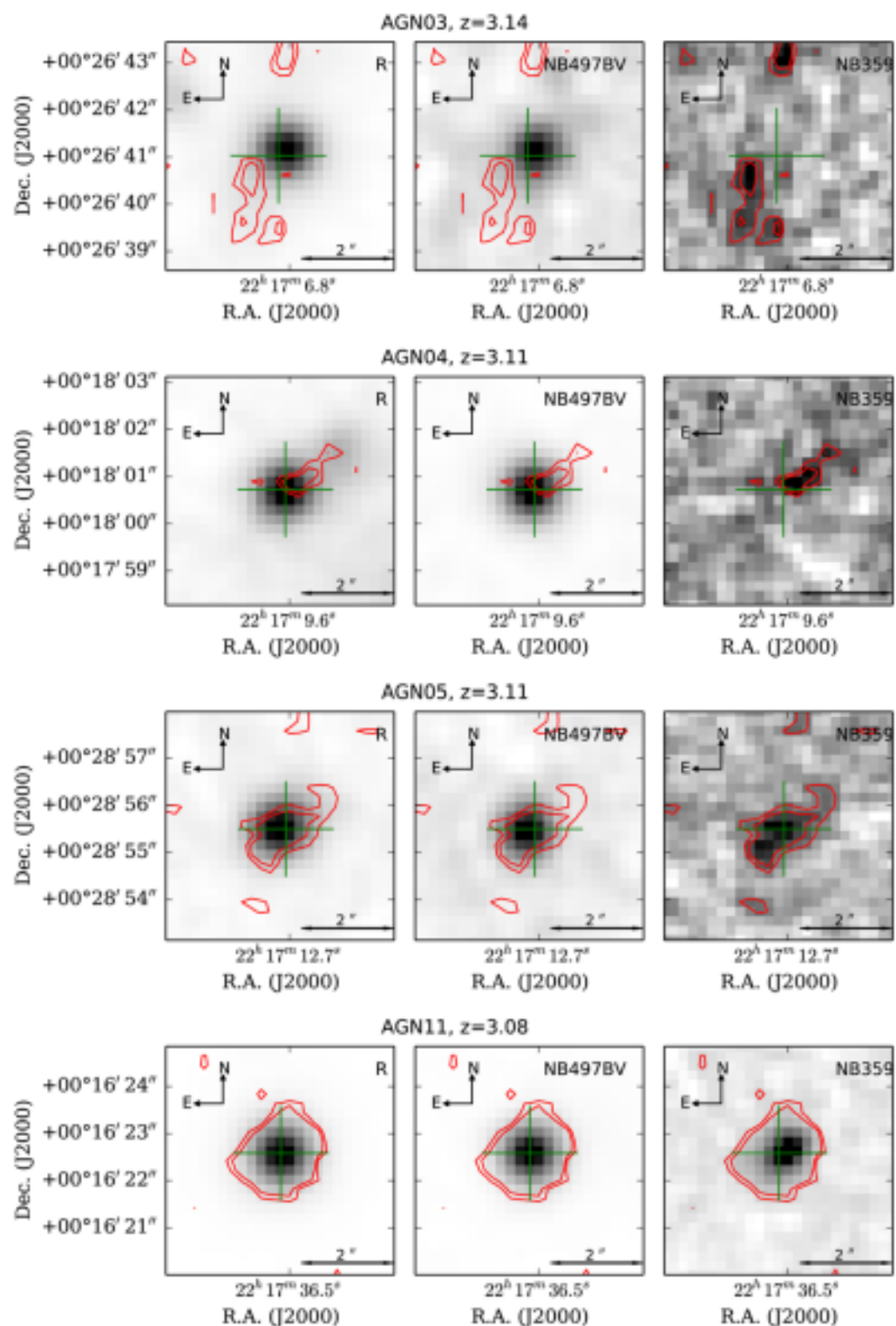
No evolution of LyC escape fraction with luminosity for $z \sim 4$ QSOs down to $M_{1450} \sim -23$.

We can assume that f_{esc} is constant also at fainter luminosities ($M_{1450} = -18$).



LyC fesc of faint AGN

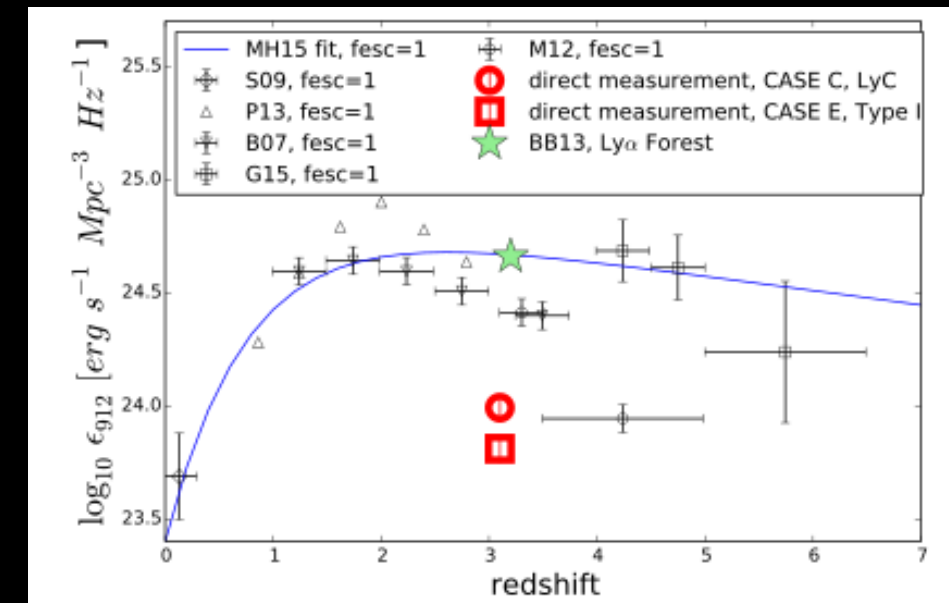
Low escape fraction of faint $z > 3$ AGN?
Fesc ~ 25%



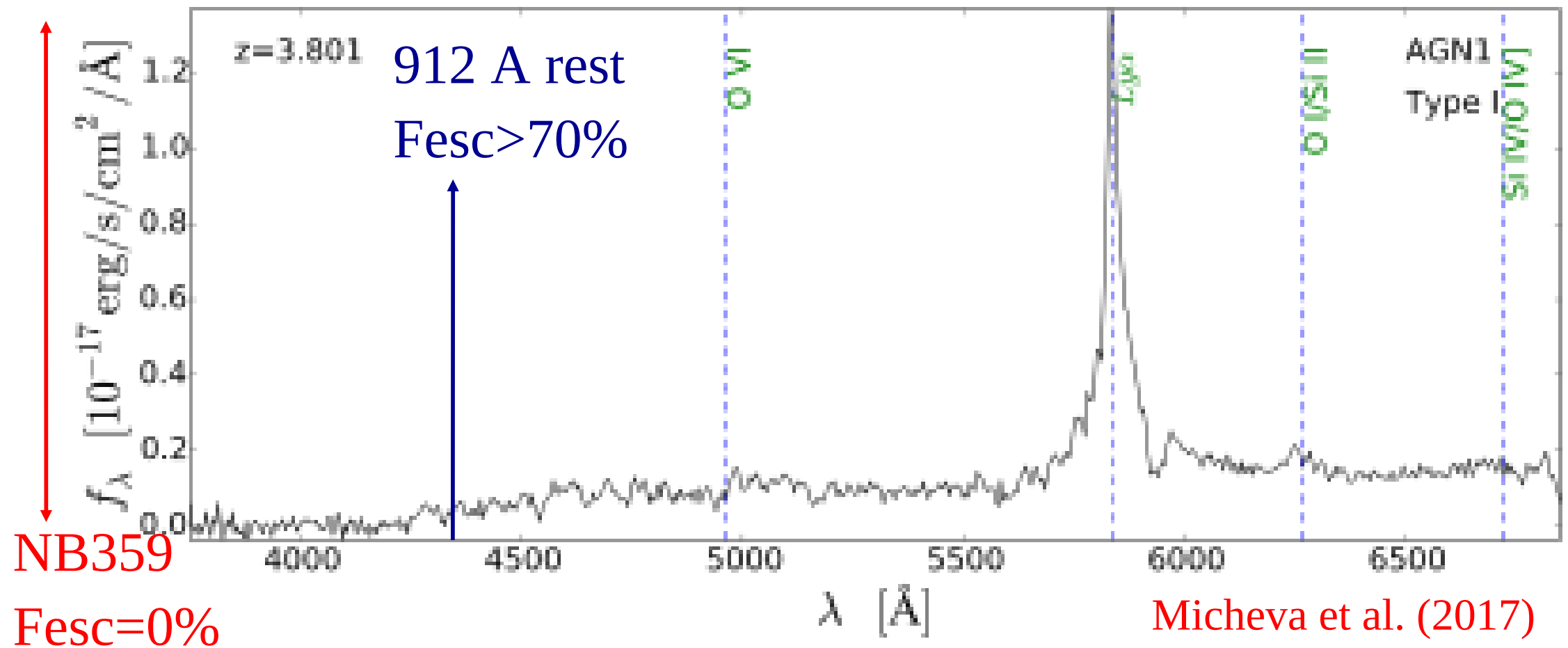
ID	FWHM	R	$R(1.2 \text{ arcsec})$	$NB359$	$NB359(1.2 \text{ arcsec})$	$(f_{1500}/f_{900})_{\text{obs}}$	$B - V$	$NB359 - R$	β (UV slope)	δr
AGN1	0.8	21.83	22.57				1.53		-1.46	
AGN2	0.8	24.75	25.52				0.69		-0.16	
AGN3	0.9	23.78	24.58	26.04 ± 0.20	28.11 ± 0.20	7.97 ± 1.42	1.18	2.25 ± 0.20	-2.47	0.8
AGN4	0.9	24.19	25.00	26.14	27.00 ± 0.12	6.06 ± 0.49	1.01	1.96	-2.41	0.5
AGN5	0.9	23.83	24.62	24.98	26.29	2.88 ± 0.19	-0.46	1.15	0.42	0.2
AGN6	0.9	24.22	25.03				0.73		-2.18	
AGN7	0.8	22.70	23.44				-0.18		-3.13	
AGN8	0.8	21.04	21.80				1.62		-2.34	
AGN9	0.9	25.91	26.79						0.76 ± 0.35	
AGN10	0.9	25.47	26.27				1.45		0.42 ± 0.17	
AGN11	0.8	21.42	22.16	24.09	24.96	11.72 ± 0.27	0.56	2.67	-1.94	0.1
AGN12	1.4	25.09	26.46				1.12		-2.39 ± 0.32	
AGN13	0.8	22.69	23.40				1.02		-0.60	
AGN14	1.2	24.53	25.69				0.87		-0.33 ± 0.18	

Micheva et al. (2017)

ID	$\lambda_{\text{eff}}^{\text{LyC}} (\text{\AA})$	$f_{\text{esc}}^{\tau=0}$	$f_{\text{esc}}^{\tau=0.32}$	$f_{\text{esc}}^{\tau=0.74}$	$\text{eH}(f_{\text{esc}})$
AGN3	867.1	<0.008	<0.011	<0.016	
AGN5	873.5	0.35	0.48	0.73	0.30
AGN7	873.9	<0.003	<0.004	<0.007	
AGN11	879.0	0.15	0.20	0.31	0.27



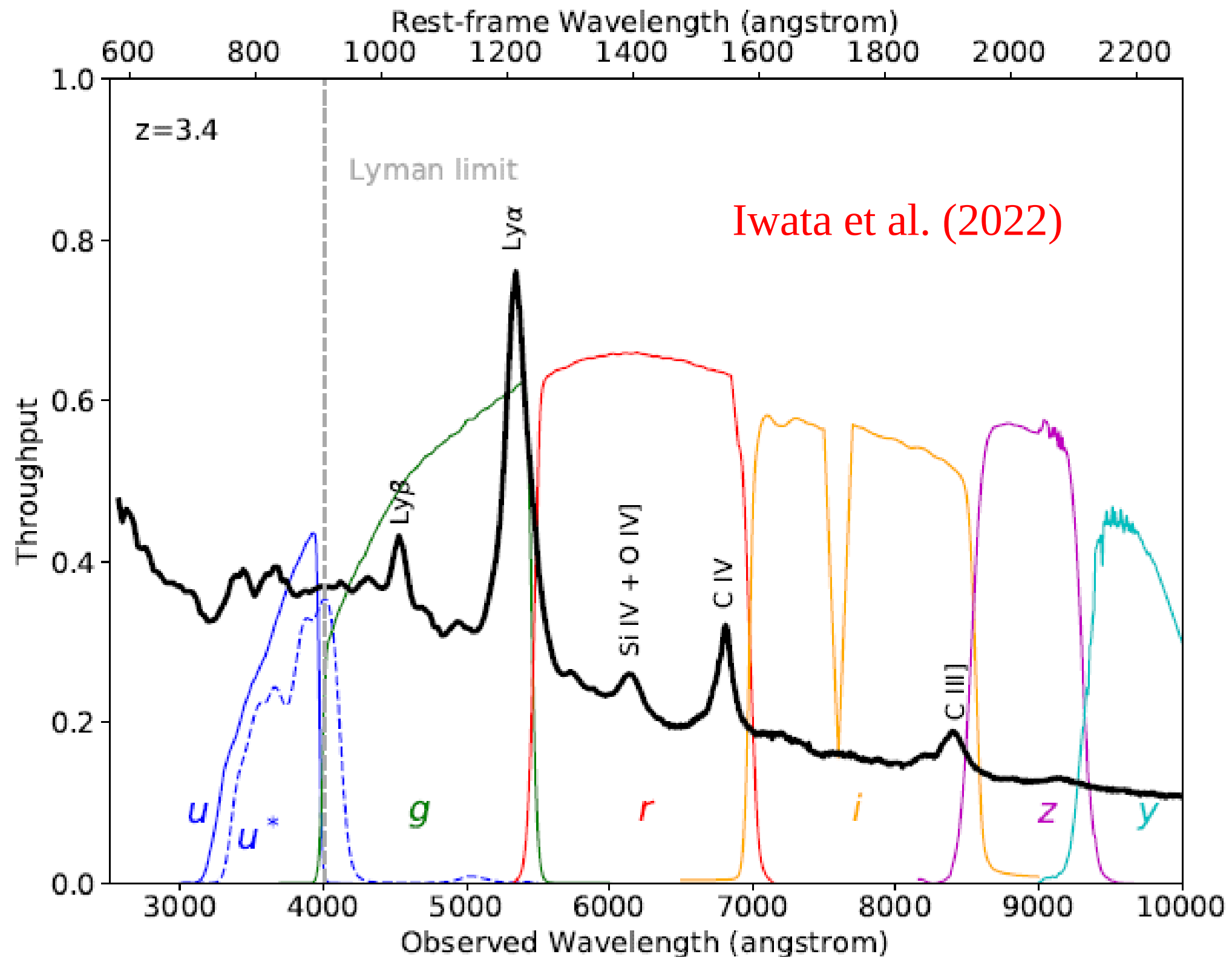
The contribution of AGNs to ionizing emissivity is 3-5 times lower than required.



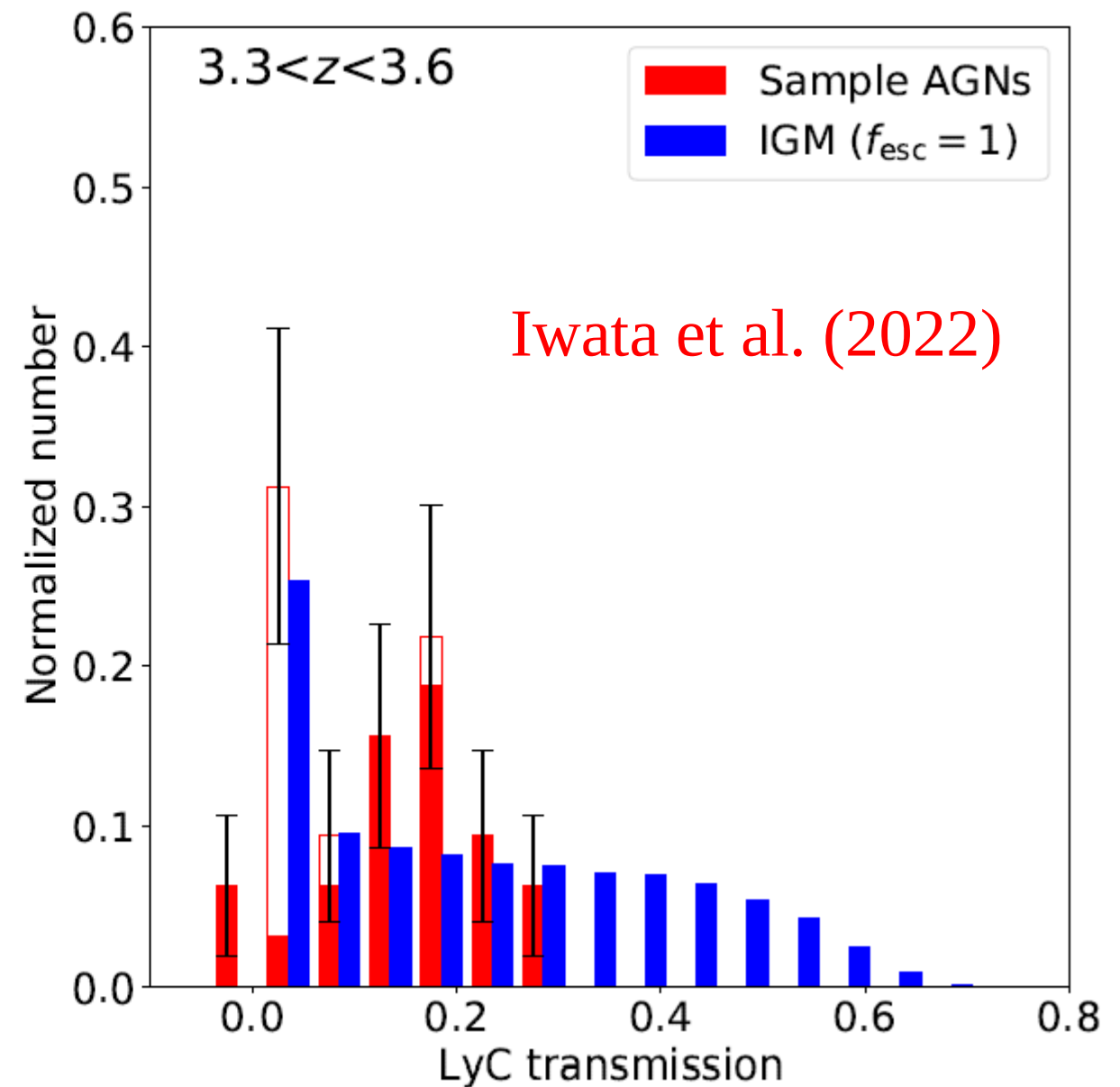
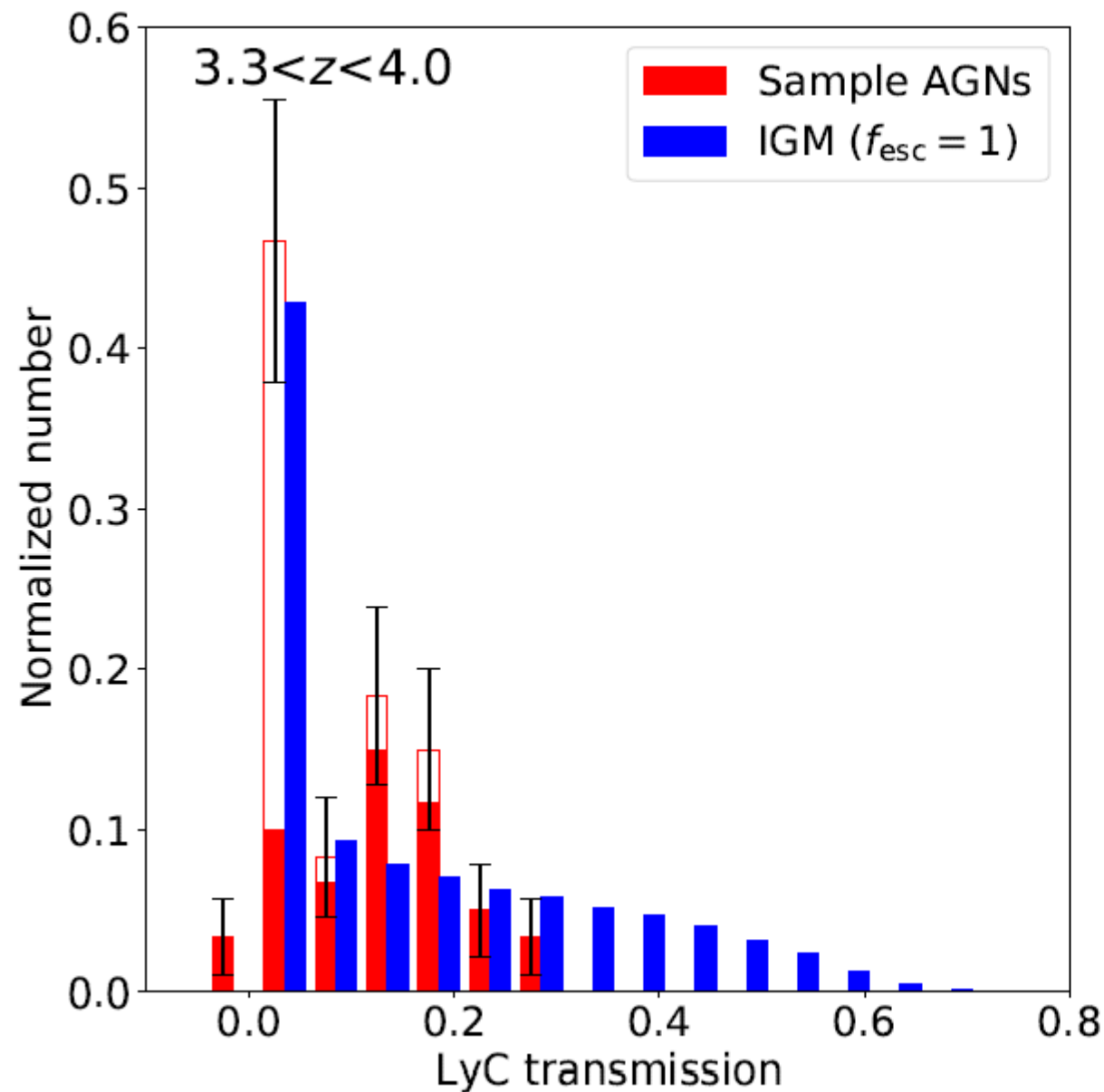
NB359 (LyC) is at 750 Å rest frame (proper distance=173 pMpc).

The Mean free path at $z=3.8$ is 45 pMpc.

Low LyC fesc of faint AGN ?



Faint High- z AGNs: low LyC f_{esc} ?



LyC $f_{\text{esc}} = 25\%$ for 94 faint ($M_{1450} > -24$) AGNs at 3.3 < z < 4.0

COSMOS

Iwata et al. (2022)

ID	R.A.(J2000)	Decl.(J2000)	Redshift	M_{1450}	$U - i$	t_{Lyc}	Filter	Type	N/E ^a	Ref. ^b	Designation
C07	149.4729034	2.7933720	3.6095	-24.127	3.18 ± 0.01	0.116 ± 0.000	<i>u</i>	BLA	N	09,09	COSMOS_J095753.49+024736.1
C08	149.5337247	1.8091995	3.9860	-23.357	> 5.54	< 0.015	<i>u</i>	-	N	10,-	B18_0664641
C10	149.6258478	1.9812633	3.9600	-20.957	2.15 ± 0.12	0.339 ± 0.013	<i>u</i>	BLA	E	11,11	L450105
C11	149.6959527	2.6030866	3.3030	-21.326	> 3.95	< -0.007	<i>u</i>	NLA	N	11,11	lid_1808
C12	149.7554065	2.7385464	3.5240	-22.169	> 4.55	< 0.032	<i>u</i>	BLA	E	12,09	COSMOS_J095901.31+024418.8
C13	149.7820781	2.4712961	3.3260	-21.819	> 4.33	< 0.003	<i>u</i>	BLA	N	11,11	L772453
C14	149.8432151	2.6590580	3.7480	-22.137	> 4.64	< 0.032	<i>u</i>	BLA	N	10,10	B18_1730531
C15	149.8457518	2.4816180	3.3600	-21.927	> 4.42	< 0.022	<i>u</i>	BLA	N	13,13	M12_1511846
C16	149.8458637	2.8604351	3.6300	-22.878	> 5.13	< 0.019	<i>u</i>	BLA	N	10,10	B18_1938843
C17	149.8494778	2.8652090	3.6860	-21.854	> 4.07	< 0.053	<i>u</i>	NLA	E	11,11	lid_2189
C18	149.8515634	2.2764026	3.3710	-22.412	2.45 ± 0.03	0.202 ± 0.001	<i>u</i>	BLA	N	12,12	XMMC_149.85099+2.27609
C19	149.8696906	2.2940175	3.3450	-23.675	> 6.24	< -0.010	<i>u</i>	BLA	N	12,12	XMMC_149.86981+2.29391
C20	149.8792145	2.2258072	3.6510	-23.017	> 5.42	< 0.015	<i>u</i>	BLA	N	12,12	XMMC_149.87949+2.22567
C21	149.8861225	2.2759378	3.3350	-21.944	> 4.52	< 0.005	<i>u</i>	NLA	E	11,11	cid_1134
C22	149.8942870	2.4329414	3.3600	-21.393	> 3.88	< 0.043	<i>u</i>	BLA	N	14,13	L747071
C23	149.9173822	2.8820631	3.3170	-21.920	2.40 ± 0.05	0.178 ± 0.006	<i>u</i>	BLA	N	14,14	L1040434
C24	150.0043858	2.0388885	3.4990	-24.064	3.24 ± 0.01	0.104 ± 0.000	<i>u</i>	BLA	N	12,12	XMMC_150.00412+2.03904
C25	150.0229091	1.5862527	3.3430	-21.297	2.49 ± 0.08	0.182 ± 0.004	<i>u</i>	NLA	E	11,11	lid_1244
C26	150.0426727	1.8721154	3.3600	-21.882	> 3.81	< 0.047	<i>u</i>	BLA	N	13,13	PRIMUS_110535
C27	150.0968272	2.0214452	3.5460	-20.424	> 2.68	< 0.180	<i>u</i>	NLA	E	15,15	CCOS1505
C28	150.1139556	2.6067261	3.9490	-20.793	> 2.72	< 0.198	<i>u</i>	BLA	E	14,14	L862385
C29	150.1164373	1.9638991	3.4100	-21.686	> 4.01	< 0.050	<i>u</i>	BLA	N	13,13	M12_0790476
C30	150.1303590	2.4659748	3.8650	-22.764	> 4.80	< 0.028	<i>u</i>	BLA	N	14,13	L768961
C31	150.2088406	2.4819033	3.3330	-25.774	> 8.15	< -0.027	<i>u</i>	BLA	N	12,12	XMMC_150.20888+2.48202
C32	150.2089844	2.4384687	3.7150	-24.470	> 6.64	< 0.005	<i>u</i>	BLA	N	12,12	XMMC_150.20929+2.43844
C33	150.2407920	2.6590184	3.3560	-22.578	2.56 ± 0.02	0.172 ± 0.001	<i>u</i>	BLA	N	12,09	XMMC_150.24087+2.65873
C34	150.2518296	1.5535407	3.7470	-21.494	> 3.31	< 0.108	<i>u</i>	BLA	N	14,14	L179154
C35	150.2595269	2.3761549	3.7170	-23.402	4.66 ± 0.10	0.031 ± 0.000	<i>u</i>	BLA	N	11,13	M12_1208399
C36	150.2630206	2.5208549	3.7580	-21.376	> 2.91	< 0.158	<i>u</i>	BLA	N	14,14	C1432719
C37	150.2671997	1.9096446	3.8460	-20.376	> 2.74	< 0.189	<i>u</i>	BLA	E	14,14	L405213
C38	150.2715836	1.6138443	3.5120	-20.122	> 2.67	< 0.177	<i>u</i>	NLA	N	11,11	cid_1656
C39	150.2972445	2.1487816	3.3280	-25.123	4.48 ± 0.01	-0.001 ± 0.007	<i>u</i>	BLA	N	12,12	XMMC_150.29764+2.14830
C40	150.3007581	2.3005428	3.4980	-21.426	> 3.98	< 0.053	<i>u</i>	NLA	E	15,15	CCOS784
C41	150.3025734	1.8520637	3.8400	-21.044	> 3.42	< 0.101	<i>u</i>	BLA	N	13,13	L368476
C42	150.3060182	1.7616025	3.3100	-20.338	> 3.01	< 0.075	<i>u</i>	NLA	E	11,11	cid_3293
C43	150.3445675	1.6359393	3.4820	-19.177	> 1.69	< 0.431	<i>u</i>	NLA	E	11,11	cid_1672
C44	150.3647089	2.1437853	3.3280	-22.050	> 3.72	< 0.032	<i>u</i>	BLA	E	14,12	L554731
C45	150.3835833	2.0747463	3.8590	-20.999	> 3.19	< 0.125	<i>u</i>	-	E	16,-	CCOS879
C46	150.3941052	2.7178277	3.4870	-21.600	1.55 ± 0.03	0.492 ± 0.006	<i>u</i>	NLA	E	11,11	lid_4112
C47	150.4029080	1.8788719	3.5710	-20.394	1.84 ± 0.08	0.393 ± 0.012	<i>u</i>	NLA	E	11,11	cid_2949
C49	150.4399178	2.7034886	3.4650	-22.510	2.79 ± 0.03	0.155 ± 0.001	<i>u</i>	BLA	N	09,09	COSMOS_J100145.58+024212.6

Fesc=74% Grazian+18

Iwata et al. (2022)

COSMOS											
ID	R.A.(J2000)	Decl.(J2000)	Redshift	M_{1450}	$U - i$	t_{lyc}	Filter	Type	N/E ^a	Ref. ^b	Designation
C07	149.4729034	2.7933720	3.6095	-24.127	3.18 ± 0.01	0.116 ± 0.000	<i>u</i>	BLA	N	09,09	COSMOS_J095753.49+024736.1
C08	149.5337247	1.8091995	3.9860	-23.357	> 5.54	< 0.015	<i>u</i>	-	N	10,-	B18_0664641
C10	149.6258478	1.9812633	3.9600	-20.957	2.15 ± 0.12	0.339 ± 0.013	<i>u</i>	BLA	E	11,11	L450105
C11	149.6959527	2.6030866	3.3030	-21.326	> 3.95	< -0.007	<i>u</i>	NLA	N	11,11	lid_1808
C12	149.7554065	2.7385464	3.5240	-22.169	> 4.55	< 0.032	<i>u</i>	BLA	E	12,09	COSMOS_J095901.31+024418.8
C13	149.7820781	2.4712961	3.3260	-21.819	> 4.33	< 0.003	<i>u</i>	BLA	N	11,11	L772453
C14	149.8432151	2.6590580	3.7480	-22.137	> 4.64	< 0.032	<i>u</i>	BLA	N	10,10	B18_1730531
C15	149.8457518	2.4816180	3.3600	-21.927	> 4.42	< 0.022	<i>u</i>	BLA	N	13,13	M12_1511846
C16	149.8458637	2.8604351	3.6300	-22.878	> 5.13	< 0.019	<i>u</i>	BLA	N	10,10	B18_1938843
C17	149.8494778	2.8652090	3.6860	-21.854	> 4.07	< 0.053	<i>u</i>	NLA	E	11,11	lid_2189
C18	149.8515634	2.2764026	3.3710	-22.412	2.45 ± 0.03	0.202 ± 0.001	<i>u</i>	BLA	N	12,12	XMMC_149.85099+2.27609
C19	149.8696906	2.2940175	3.3450	-23.675	> 6.24	< -0.010	<i>u</i>	BLA	N	12,12	XMMC_149.86981+2.29391
C20	149.8792145	2.2258072	3.6510	-23.017	> 5.42	< 0.015	<i>u</i>	BLA	N	12,12	XMMC_149.87949+2.22567
C21	149.8861225	2.2759378	3.3350	-21.944	> 4.52	< 0.005	<i>u</i>	NLA	E	11,11	cid_1134
C22	149.8942870	2.4329414	3.3600	-21.393	> 3.88	< 0.043	<i>u</i>	BLA	N	14,13	L747071
C23	149.9173822	2.8820631	3.3170	-21.920	2.40 ± 0.05	0.178 ± 0.006	<i>u</i>	BLA	N	14,14	L1040434
C24	150.0043858	2.0388885	3.4990	-24.064	3.24 ± 0.01	0.104 ± 0.000	<i>u</i>	BLA	N	12,12	XMMC_150.00412+2.03904
C25	150.0229091	1.5862527	3.3430	-21.297	2.49 ± 0.08	0.182 ± 0.004	<i>u</i>	NLA	E	11,11	lid_1244
C26	150.0426727	1.8721154	3.3600	-21.882	> 3.81	< 0.047	<i>u</i>	BLA	N	13,13	PRIMUS_110535
C27	150.0968272	2.0214452	3.5460	-20.424	> 2.68	< 0.180	<i>u</i>	NLA	E	15,15	CCOS1505
C28	150.1139556	2.6067261	3.9490	-20.793	> 2.72	< 0.198	<i>u</i>	BLA	E	14,14	L862385
C29	150.1164373	1.9638991	3.4100	-21.686	> 4.01	< 0.050	<i>u</i>	BLA	N	13,13	M12_0790476
C30	150.1303590	2.4659748	3.8650	-22.764	> 4.80	< 0.028	<i>u</i>	BLA	N	14,13	L768961
C31	150.2088406	2.4819033	3.3330	-25.774	> 8.15	< -0.027	<i>u</i>	BLA	N	12,12	XMMC_150.20888+2.48202
C32	150.2089844	2.4384687	3.7150	-24.470	> 6.64	< 0.005	<i>u</i>	BLA	N	12,12	XMMC_150.20929+2.43844
C33	150.2407920	2.6590184	3.3560	-22.578	2.56 ± 0.02	0.172 ± 0.001	<i>u</i>	BLA	N	12,09	XMMC_150.24087+2.65873
C34	150.2518296	1.5535407	3.7470	-21.494	> 3.31	< 0.108	<i>u</i>	BLA	N	14,14	L179154
C35	150.2595269	2.3761549	3.7170	-23.402	4.66 ± 0.10	0.031 ± 0.000	<i>u</i>	BLA	N	11,13	M12_1208399
C36	150.2630206	2.5208549	3.7580	-21.376	> 2.91	< 0.158	<i>u</i>	BLA	N	14,14	C1432719
C37	150.2671997	1.9096446	3.8460	-20.376	> 2.74	< 0.189	<i>u</i>	BLA	E	14,14	L405213
C38	150.2715836	1.6138443	3.5120	-20.122	> 2.67	< 0.177	<i>u</i>	NLA	N	11,11	cid_1656
C39	150.2972445	2.1487816	3.3280	-25.123	4.48 ± 0.01	-0.001 ± 0.007	<i>u</i>	BLA	N	12,12	XMMC_150.29764+2.14830
C40	150.3007581	2.3005428	3.4980	-21.426	> 3.98	< 0.053	<i>u</i>	NLA	E	15,15	CCOS784
C41	150.3025734	1.8520637	3.8400	-21.844	> 3.42	< 0.101	<i>u</i>	BLA	N	13,13	L368476
C42	150.3060182	1.7616025	3.3100	-20.338	> 3.01	< 0.075	<i>u</i>	NLA	E	11,11	cid_3293
C43	150.3445675	1.6359393	3.4820	-19.177	> 1.69	< 0.431	<i>u</i>	NLA	E	11,11	cid_1672
C44	150.3647089	2.1437853	3.3280	-22.050	> 3.72	< 0.032	<i>u</i>	BLA	E	14,12	L554731
C45	150.3835833	2.0747463	3.8590	-20.999	> 3.19	< 0.125	<i>u</i>	-	E	16,-	CCOS879
C46	150.3941052	2.7178277	3.4870	-21.600	1.55 ± 0.03	0.492 ± 0.006	<i>u</i>	NLA	E	11,11	lid_4112
C47	150.4029080	1.8788719	3.5710	-20.394	1.84 ± 0.08	0.393 ± 0.012	<i>u</i>	NLA	E	11,11	cid_2949
C49	150.4399178	2.7034886	3.4650	-22.510	2.79 ± 0.03	0.155 ± 0.001	<i>u</i>	BLA	N	09,09	COSMOS_J100145.58+024212.6

Fesc=51% Grazian+18

Fesc=51% Grazian+18

Fesc=78% Grazian+18

COSMOS											Iwata et al. (2022)
ID	R.A.(J2000)	Decl.(J2000)	Redshift	M_{1450}	$U - i$	t_{Lyc}	Filter	Type	N/E ^a	Ref. ^b	Designation
C50	150.4549406	1.9673839	3.4710	-21.548	> 3.96	< 0.053	<i>u</i>	BLA	N	11,11	L441487
C51	150.5508002	2.6828885	3.5600	-21.818	> 4.11	< 0.048	<i>u</i>	BLA	N	13,13	M12_1628943
C52	150.6384404	2.3913200	3.6500	-23.195	> 5.04	< 0.021	<i>u</i>	BLA	N	13,13	M12_1159815
C53	150.7037829	2.3699723	3.7490	-23.966	3.28 ± 0.02	0.112 ± 0.000	<i>u</i>	BLA	N	12,12	XMMC_150.70394+2.36961
C54	150.7170733	1.9301231	3.5675	-22.732	1.23 ± 0.01	0.694 ± 0.003	<i>u</i>	BLA	E	11,11	L419634
C55	150.7355581	2.1995513	3.4970	-25.257	3.14 ± 0.00	0.063 ± 0.006	<i>u</i> *	BLA	N	11,12	lid_1710
C56	150.7371767	2.7225658	3.3020	-23.399	2.29 ± 0.01	0.186 ± 0.009	<i>u</i>	BLA	N	12,09	COSMOS_J100256.92+024321.2
C57	150.7822171	2.2850682	3.6260	-23.993	3.79 ± 0.03	0.046 ± 0.001	<i>u</i> *	BLA	N	10,10	B18_0899256
C59	150.8013187	1.6574845	3.7720	-23.212	> 5.63	< 0.013	<i>u</i>	-	N	10,-	B18_0247934
C60	150.9112639	1.9448424	3.6800	-24.963	4.43 ± 0.02	0.038 ± 0.000	<i>u</i>	BLA	N	03,03	VVDSWIDE:100359356
C61	150.9430180	1.3197523	3.5570	-24.265	> 6.63	< 0.005	<i>u</i>	BLA	N	03,03	VVDSWIDE:100105943
C62	151.2614791	1.4073308	3.4035	-25.349	3.07 ± 0.00	0.117 ± 0.000	<i>u</i>	BLA	N	02,02	SDSS100502.75+012426.3

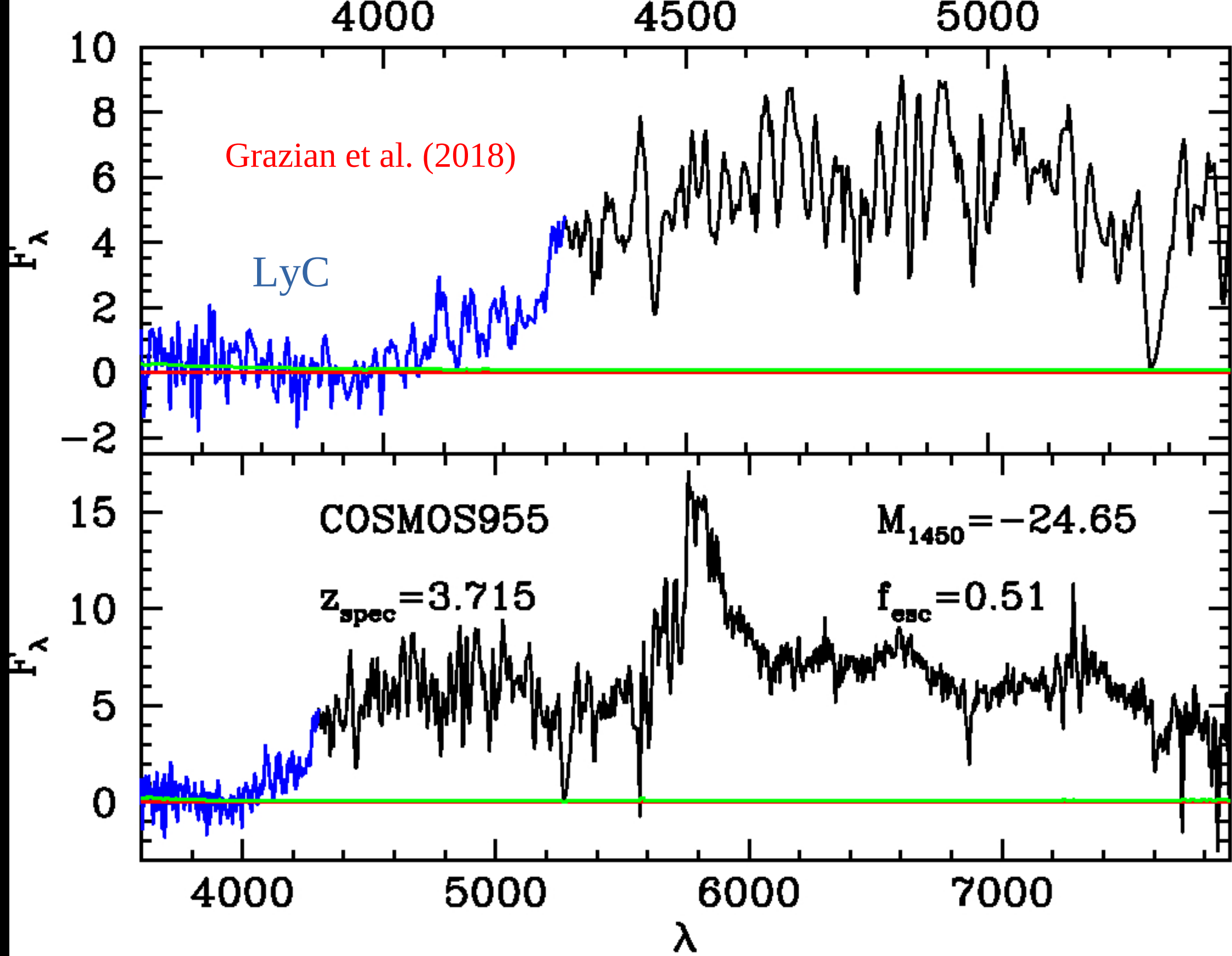
Name Iwata+22 Grazian+18

C07 fesc=19% fesc=74%

C32 fesc<1% fesc=51%

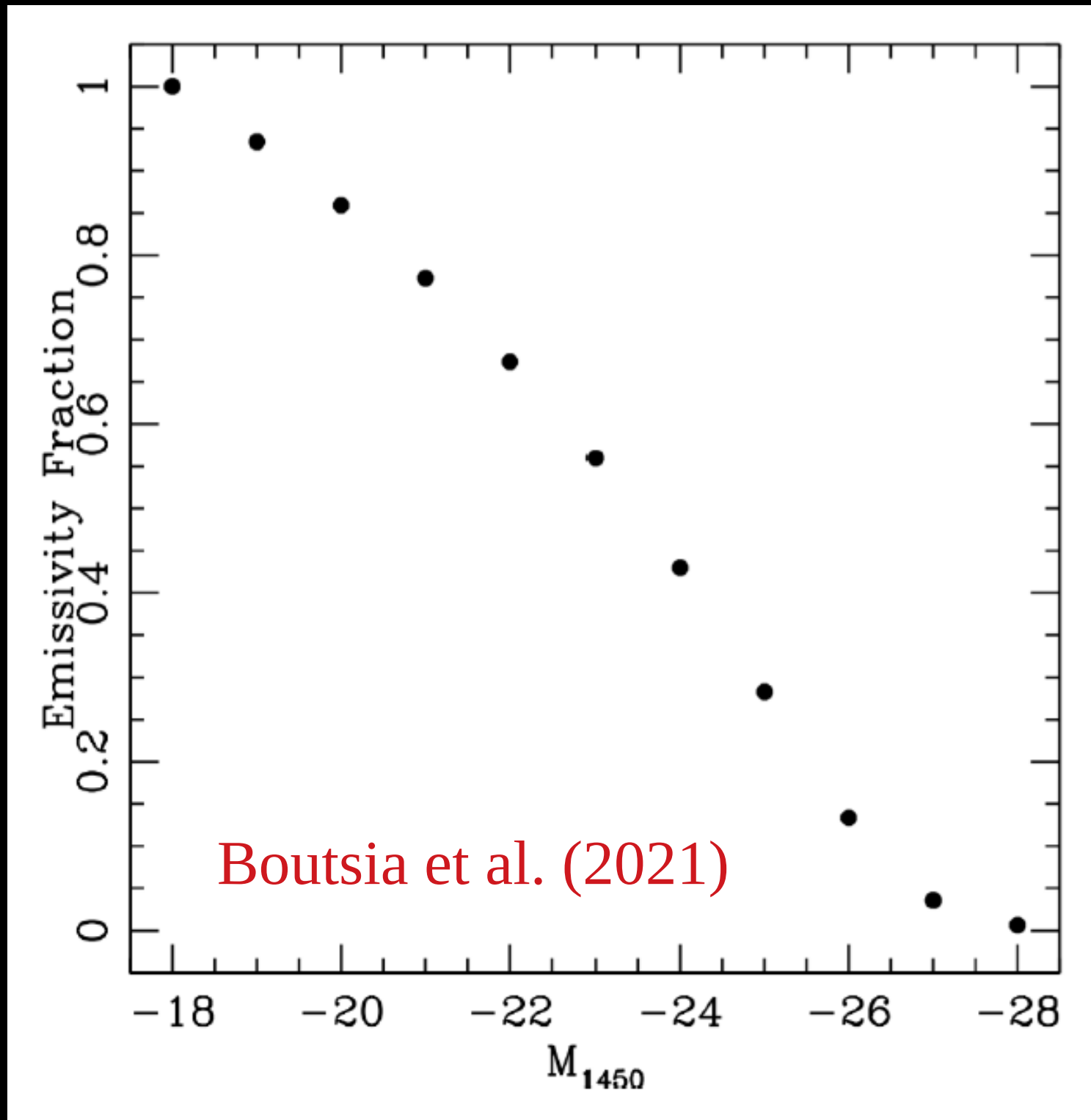
C35 fesc=5% fesc=51%

C53 fesc=18% fesc=78%



Name Iwata+22 Grazian+18
C32 $f_{\text{esc}} < 1\%$ $f_{\text{esc}} = 51\%$

The bulk (more than 50%) of the ionizing luminosity density is produced by AGNs brighter than $M_{1450} = -23$, close to L^* .



Implications for a strong LyC escape fraction of high- z AGNs: a simple model.

Based on Madau et al. (2024)

Model assumptions - A

(a) the fraction of broad-line type-1 AGNs among galaxies is around 10-15%;

Table 4

Fraction and Number Densities of Our Broad-line AGNs

M_{UV} (mag)	f_{AGN}
	$z \sim 4$ ($z_{avg} = 4.365$)
-21.5	$0.07^{+0.15}_{-0.06}$
-18.5	$0.15^{+0.15}_{-0.09}$
	$z \sim 5$ ($z_{avg} = 4.912$)
-21.5	<0.10
-18.5	$0.04^{+0.05}_{-0.02}$
	$z \sim 6$ ($z_{avg} = 5.763$)
-21.5	$0.07^{+0.17}_{-0.06}$
-18.5	$0.04^{+0.10}_{-0.04}$
	$z \sim 7$ ($z_{avg} = 6.936$)
-21.5	$0.07^{+0.17}_{-0.06}$
-18.5	<0.19

Note. Errors are 1σ and upper limits are 2σ .

Harikane et al.
(2023)

JADES. The diverse population of infant Black Holes at $4 < z < 11$: merging, tiny, poor, but mighty

Roberto Maiolino^{1,2,3,*}, Jan Scholtz^{1,2}, Emma Curtis-Lake⁴, Stefano Carniani⁵, William Baker^{1,2}, Anna de Graaff⁶, Sandro Tacchella^{1,2}, Hannah Übler^{1,2}, Francesco D'Eugenio^{1,2}, Joris Witstok^{1,2}, Mirko Curti⁷, Santiago Arribas⁸, Andrew J. Bunker⁹, Stéphane Charlot¹⁰, Jacopo Chevallard⁹, Daniel J. Eisenstein¹¹, Eiichi Egami¹², Zhiyuan Ji¹², Gareth C. Jones⁹, Jianwei Lyu¹², Tim Rawle¹³, Brant Robertson¹⁴, Wiphu Rujopakarn¹⁵, Michele Perna⁸, Fengwu Sun¹², Giacomo Venturi⁵, Christina C. Williams¹⁶, and Chris Willott¹⁷

(Affiliations can be found after the references)

Maiolino et al. (2024)

ABSTRACT

Spectroscopy with the James Webb Space Telescope has opened the possibility to identify moderate luminosity Active Galactic Nuclei (AGN) in the early Universe, at and beyond the epoch of reionization, complementing previous surveys of much more luminous (and much rarer) quasars. We present 12 new AGN at $4 < z < 7$ in the JADES survey (in addition to the previously identified AGN in GN-z11 at $z=10.6$) revealed through the detection of a Broad Line Region as seen in the Balmer emission lines. The depth of JADES, together with the use of three different spectral resolutions, enables us to probe a lower mass regime relative to previous studies. In a few cases we find evidence for two broad components of $H\alpha$, which suggests that these could be candidate merging black holes (BHs). The inferred BH masses range between $8 \times 10^7 M_\odot$ down to $4 \times 10^5 M_\odot$, interestingly probing the regime expected for Direct Collapse Black Holes. The inferred AGN bolometric luminosities ($\sim 10^{44} - 10^{45}$ erg/s) imply accretion rates that are < 0.5 times the Eddington rate in most cases. However, small BHs, with $M_{BH} \sim 10^6 M_\odot$, tend to accrete at Eddington or super-Eddington rates. These BHs at $z \sim 4-11$ are over-massive relative to their host galaxies stellar masses when compared to the local $M_{BH} - M_{star}$ relation, even approaching $M_{BH} \sim M_{star}$, as expected from heavy BH seeds and/or super-Eddington accretion scenarios. However, we find that these early BH tend to be more consistent with the local relation between M_{BH} and velocity dispersion, as well as between M_{BH} and dynamical mass, suggesting that these are more fundamental and universal relations. On the BPT excitation-diagnostic diagram these AGN are located in the region that is that is locally occupied by star-forming galaxies, implying that they would be missed by the standard classification techniques if they did not display broad lines. Their location on the diagram is consistent with what expected for AGN hosted in metal poor galaxies ($Z \sim 0.1 - 0.2 Z_\odot$). The fraction of broad line AGN with $L_{AGN} > 10^{44}$ erg/s among galaxies in the redshift range $4 < z < 6$ is about 10%, suggesting that the contribution of AGN and their hosts to the reionization of the Universe is $> 10\%$.

Key words. Galaxies: active - Galaxies: high-redshift - Galaxies: luminosity function - quasars: general

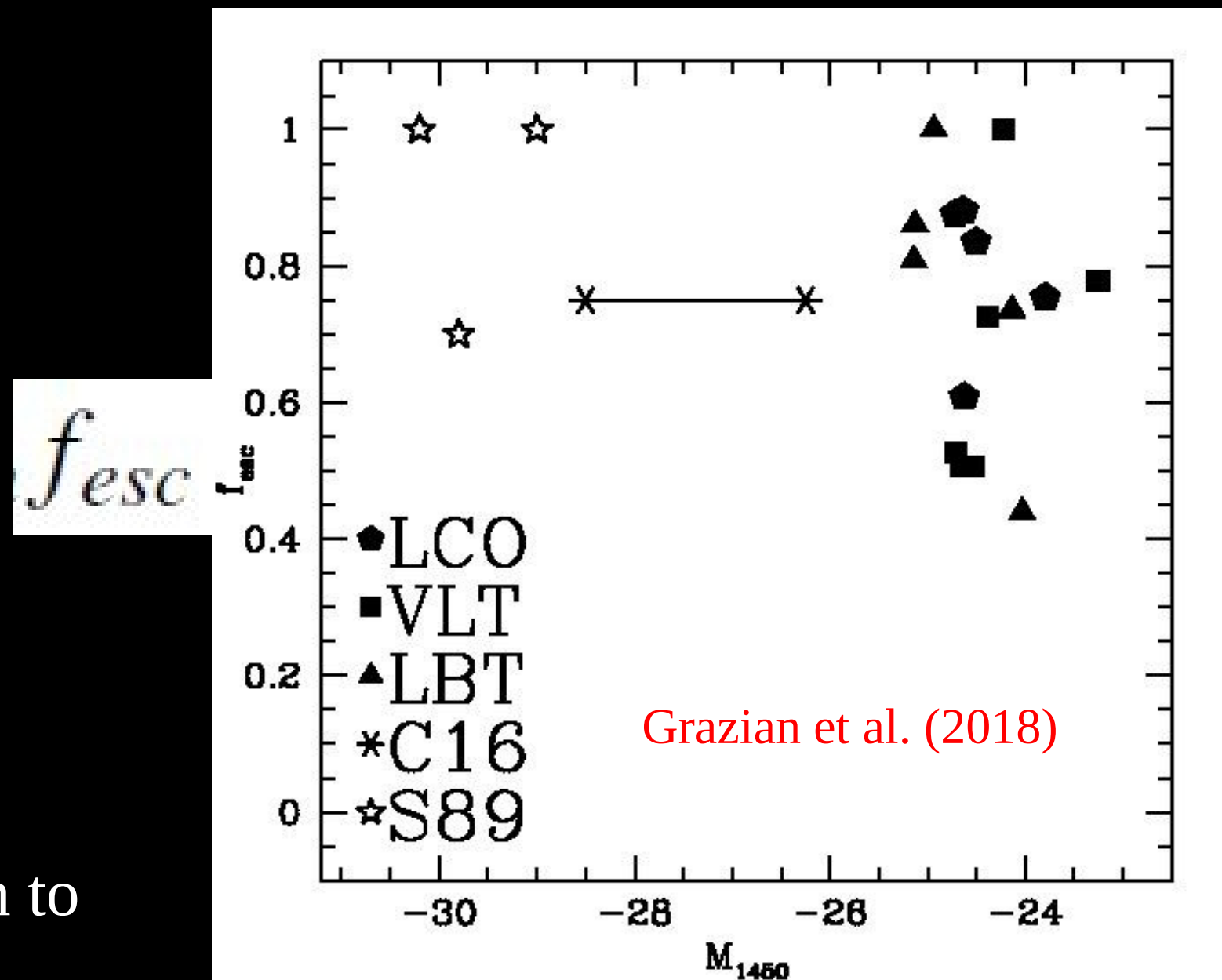
Model assumptions - B

(b) the mean escape fraction of hydrogen LyC radiation is high, $>80\%$, in AGN hosts and is negligible otherwise;

~ 1600 QSOs $M_{1450} = -26$
($L \sim 5L^*$) have average
 $f_{\text{esc}} \sim 75\%$ (or more). See
Cristiani et al. (2016) and
Romano et al. (2019).

No dependence of
LyC f_{esc} from
Luminosity has been
detected

LARGE LYC ESCAPE
FRACTION for AGNs, down to
 $M_{1450} = -23$ at $z \sim 4$













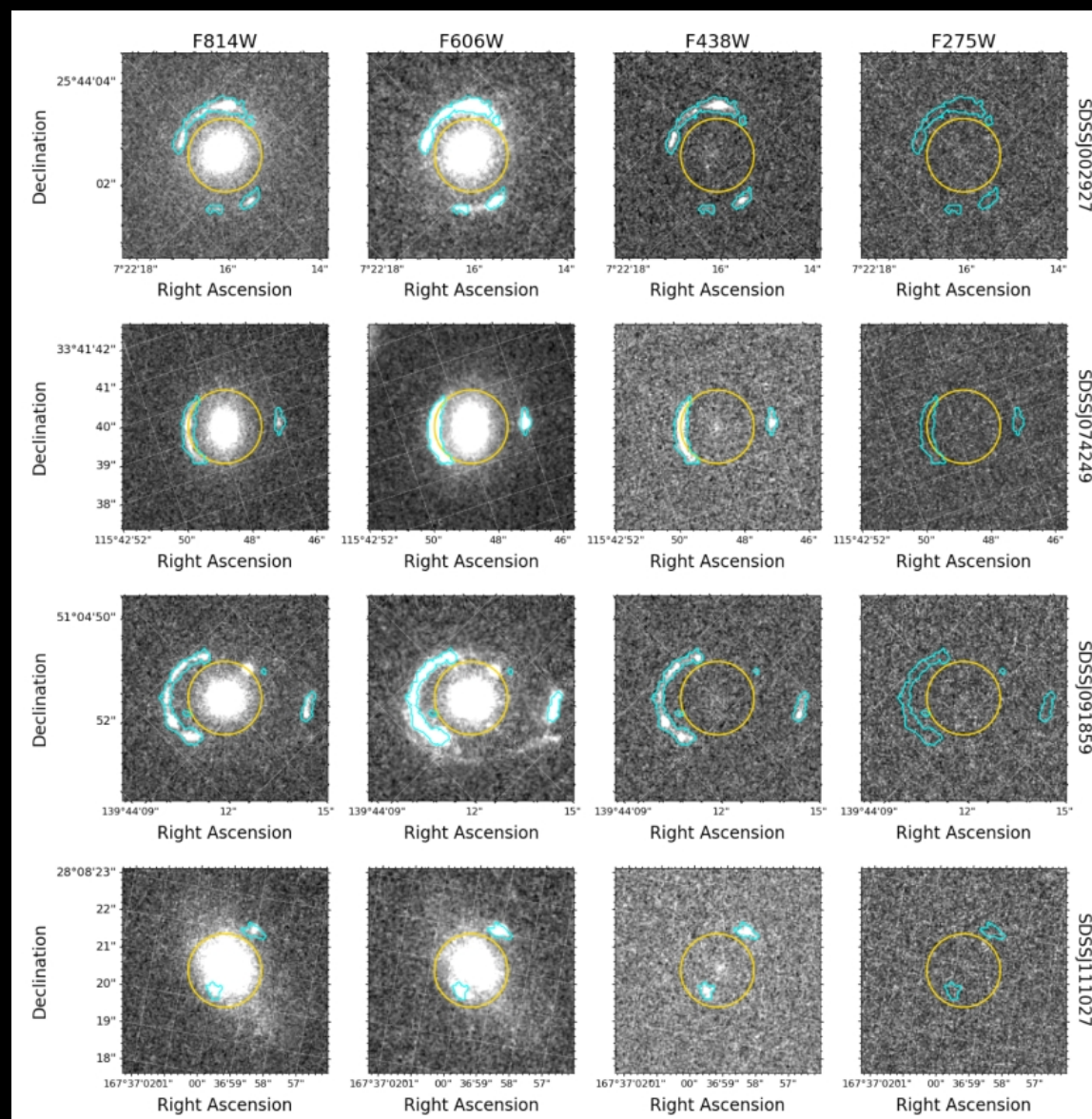
Model assumptions - B

(b) the mean escape fraction of hydrogen LyC radiation is high, $>80\%$, in AGN hosts and is negligible otherwise;

Citro et al. (2024)

Challenging the LyC – Ly α relation: strong Ly α emitters without LyC leakage at $z \sim 2.3$

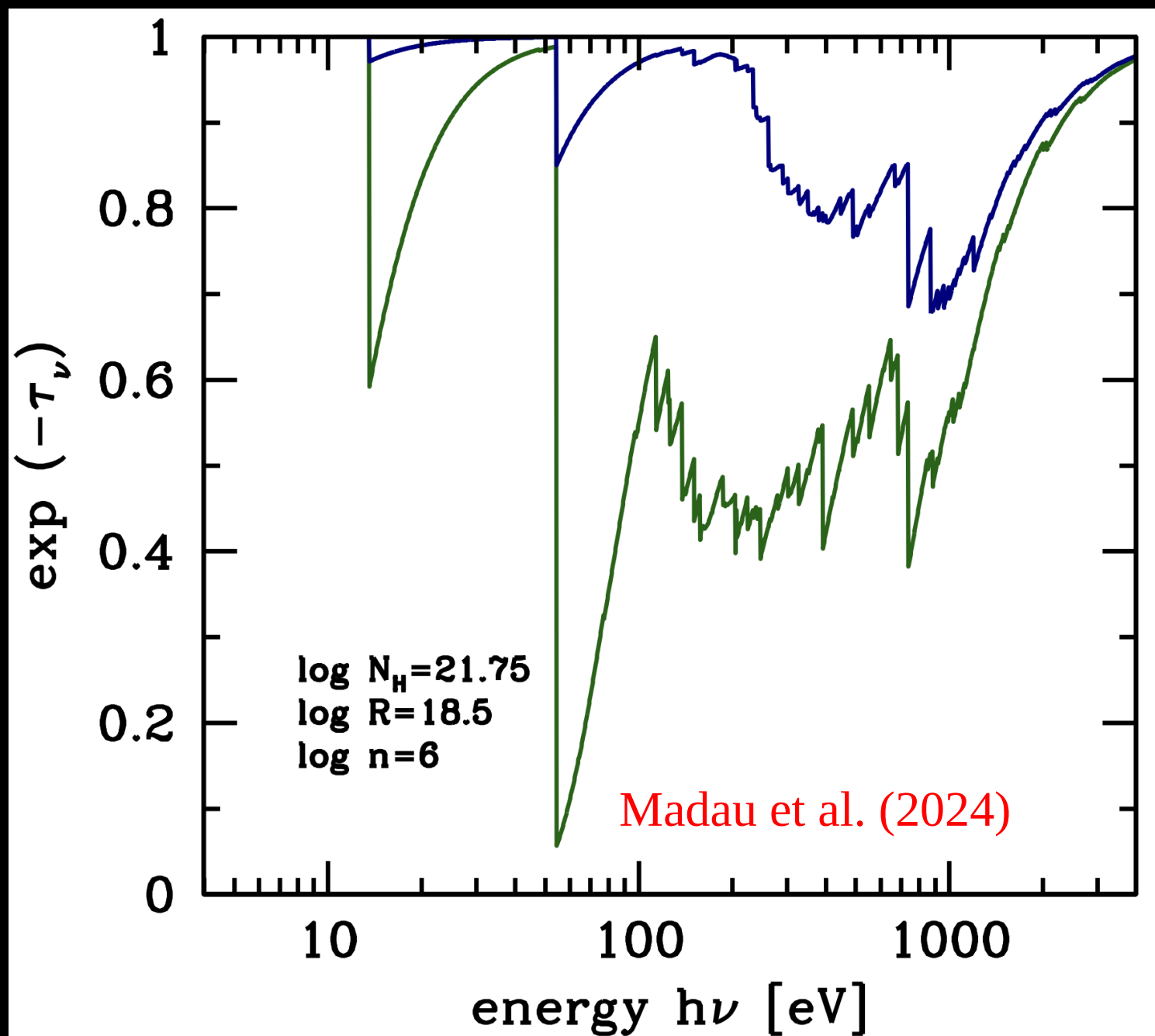
ANNALISA CITRO ¹ CLAUDIA M. SCARLATA ¹ KAMESWARA B. MANTHA ¹ LILIYA R. WILLIAMS ¹
MARC RAFELSKI ^{2,3} MITCHELL REVALSKI ² MATTHEW J. HAYES ⁴ ALAINA HENRY ² MICHAEL J. RUTKOWSKI ⁵
AND HARRY I. TEPLITZ ⁶



7 Lensed Star Forming galaxies
at $z \sim 2.3$ and $-21 < M_{\text{UV}} < -19$:
Absolute $f_{\text{esc}} < 6.5\%$ (at 3
sigma). See talk by Intae Jung
and paper by Citro et al. (2024).

Model assumptions - C

(c) internal absorption at 4 Ryd or a steep ionizing EUV spectrum delay full reionization of HeII until $z=2.8-3.0$, in agreement with observations of the HeII Lyman-alpha forest.



(MUV, α EUV) = (-19.5, -1.8)

$F_{\text{esc,H}}=0.99$

$F_{\text{esc,He}}=0.93$

(MUV, α EUV) = (-18.5, -1.4)

$F_{\text{esc,H}}=0.82$

$F_{\text{esc,He}}=0.33$

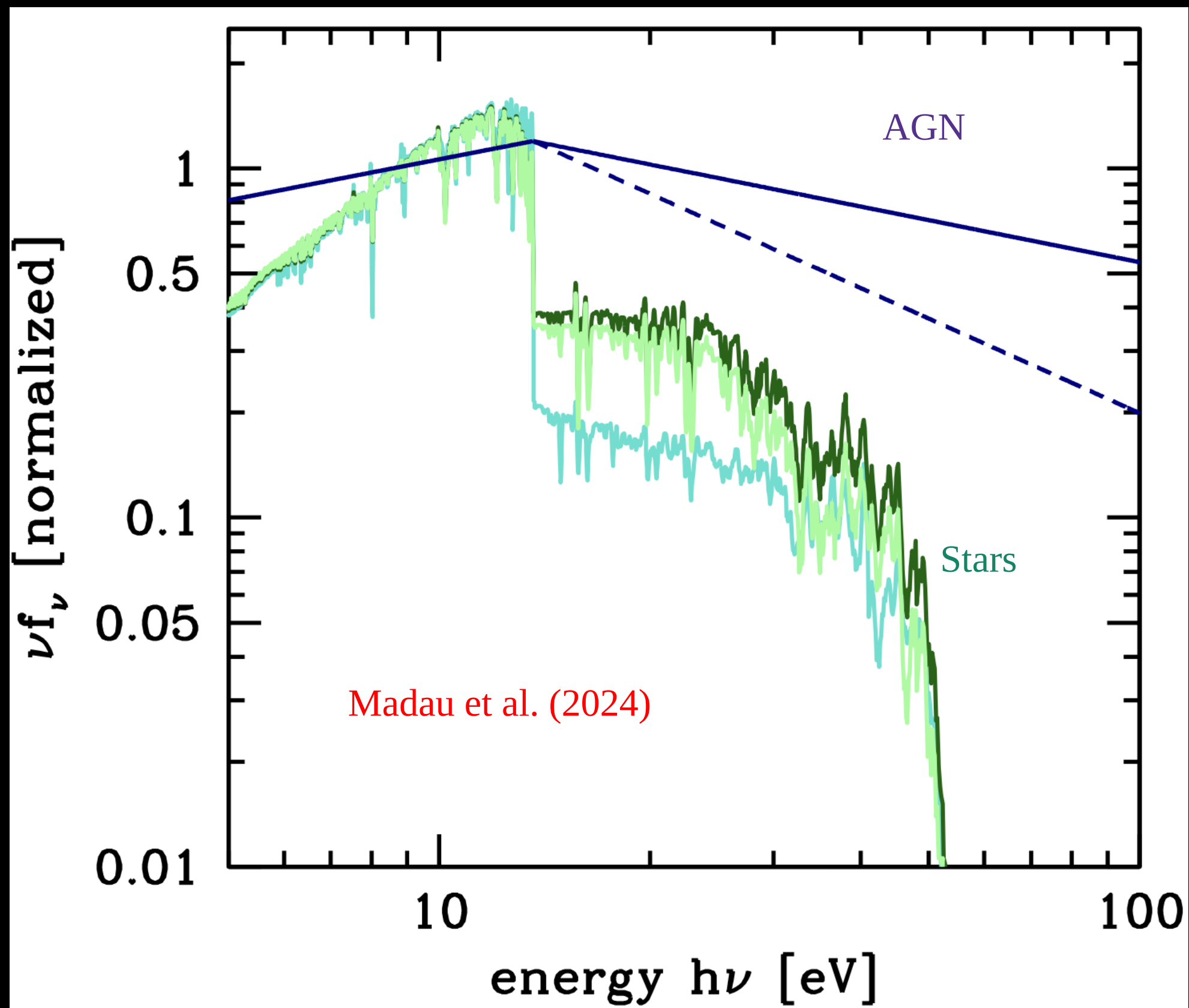
Sub-parsec absorption
(between BLR and disk)

Madau et al. (2024)

arXiv:2406.18697

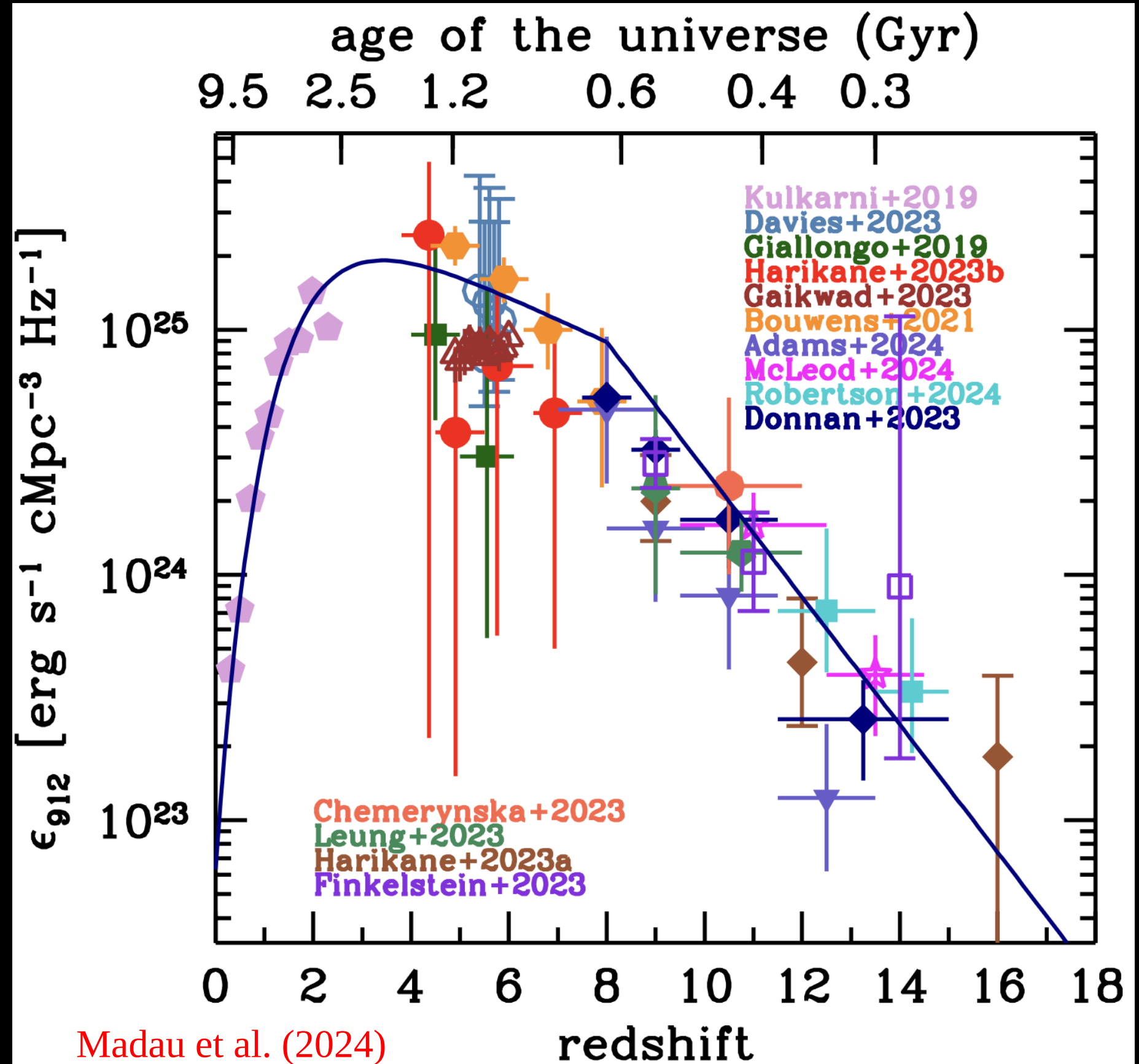
CLOUDY

(Ferland et al. 2017)



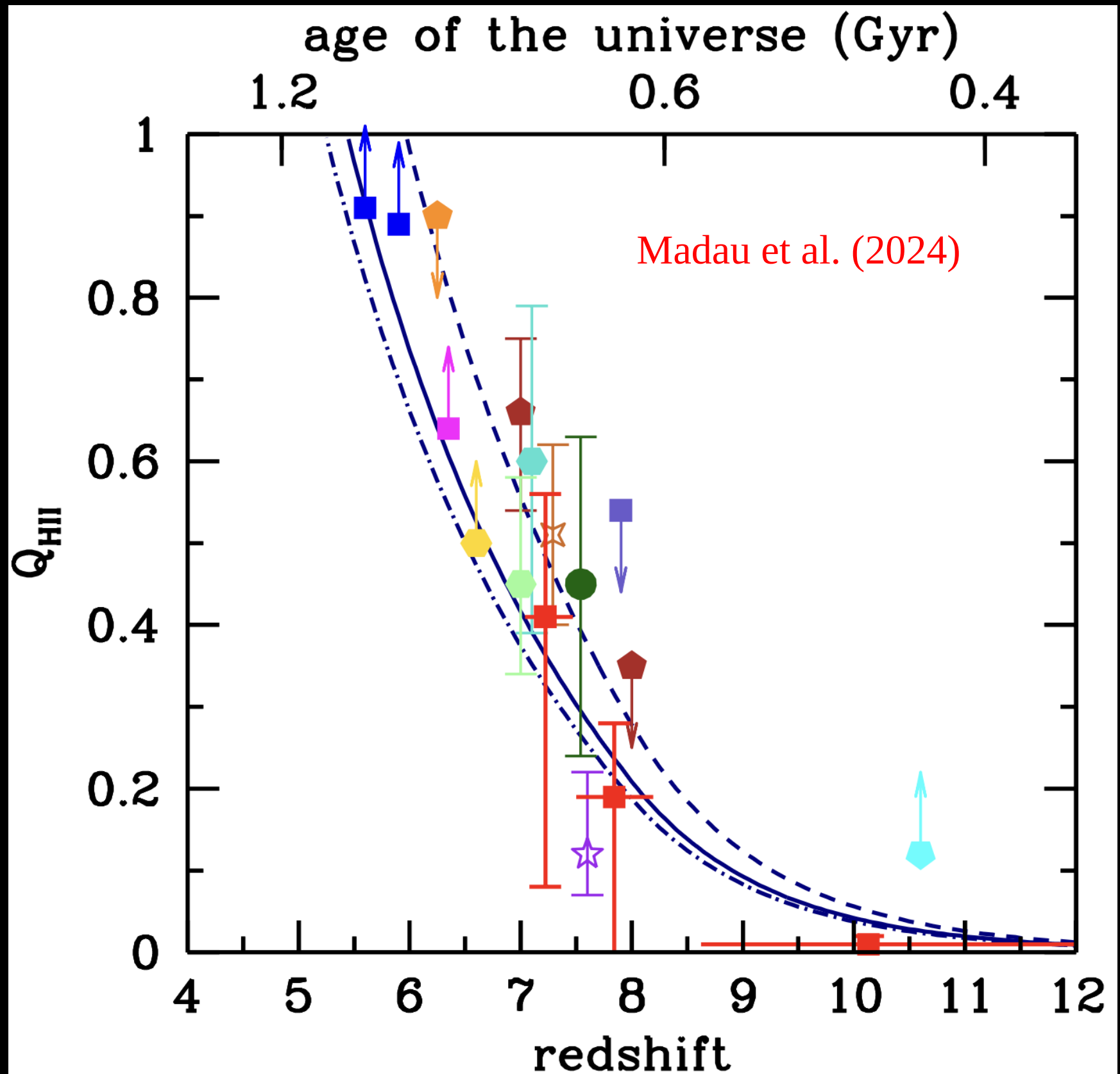
Results

The HI ionizing
Emissivity of the
model matches
the results of a
number of works.



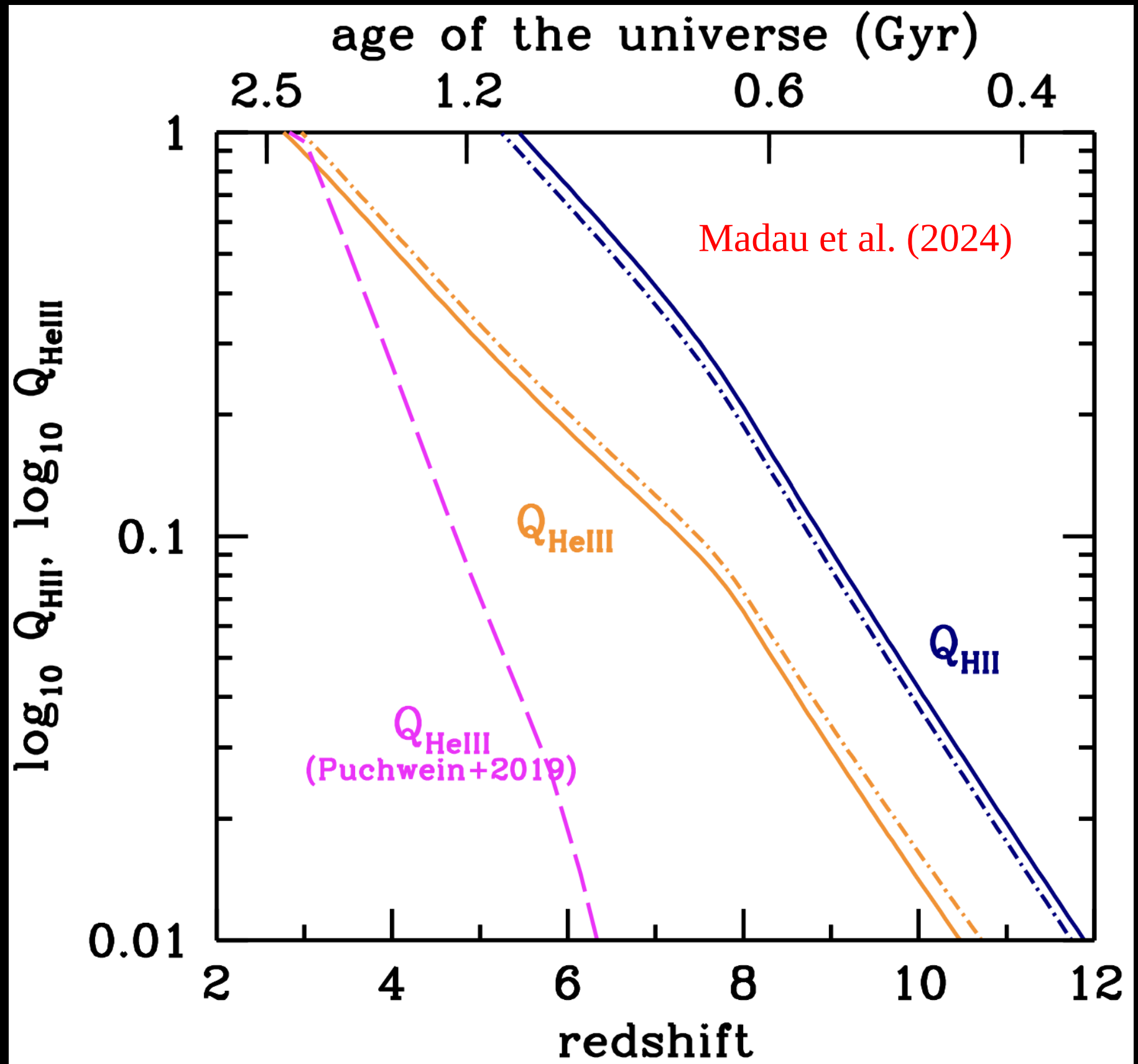
Results

The evolving HII ionizing volume filling fraction of the model matches the collection of results from the literature.



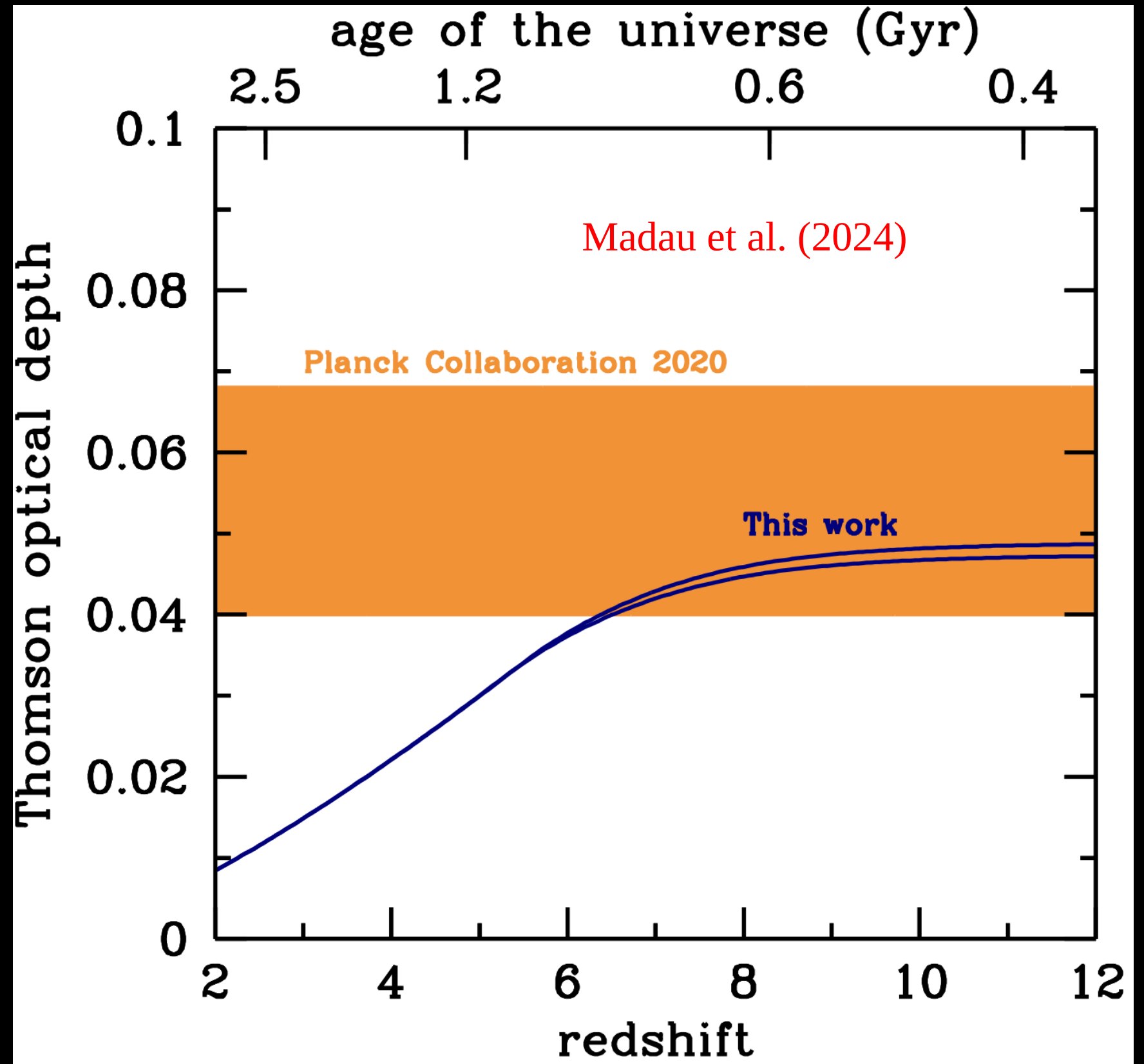
Results

The hydrogen reionization is 99% completed by redshift $z=5.3-5.5$, and reaches its midpoint at $z=6.5-6.7$. HeII reionization ends at redshift $z\sim 3$.



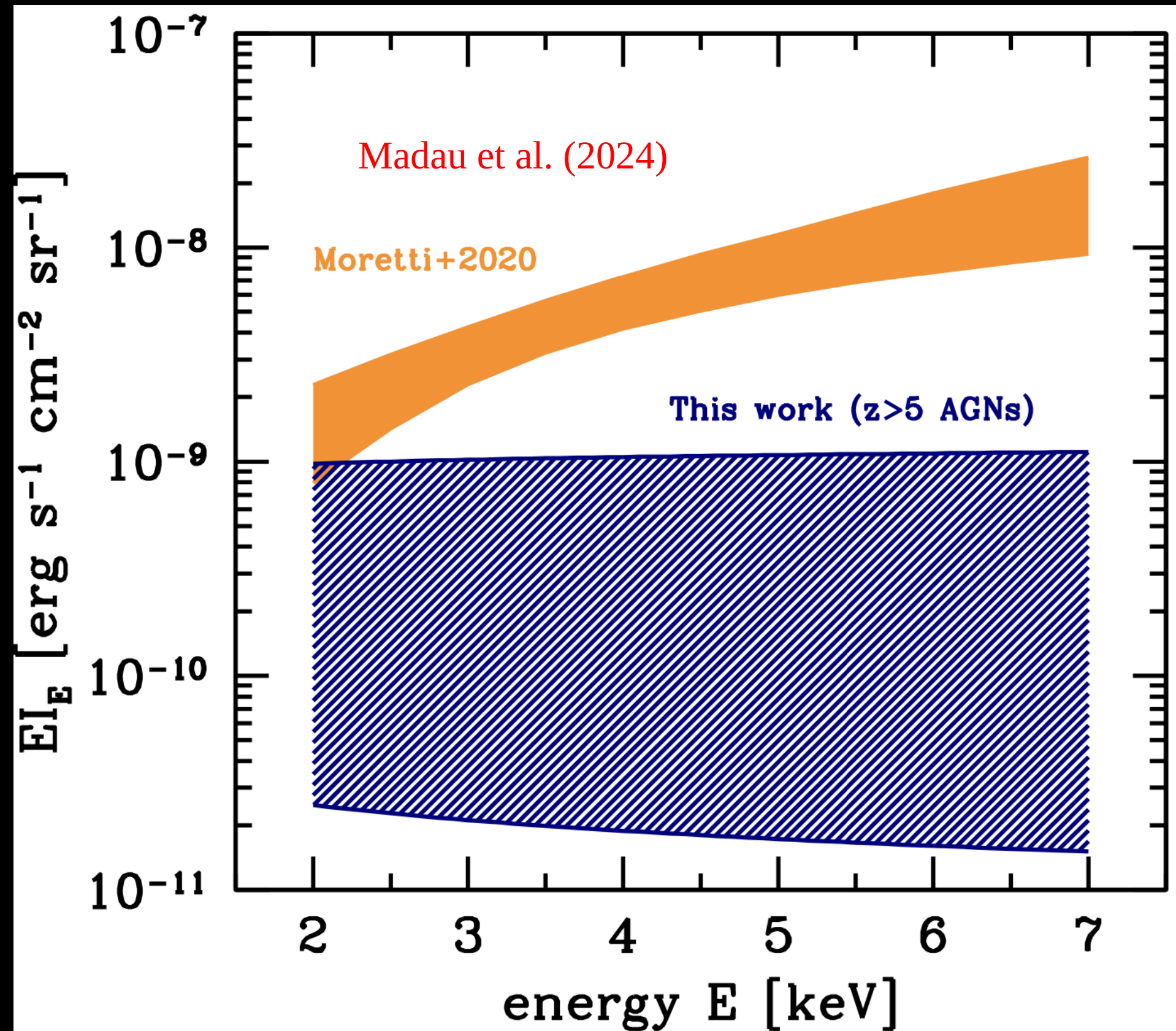
Results

The integrated Thomson scattering optical depth to reionization is $\tau=0.05$, consistent with constraints from cosmic microwave background (CMB) anisotropy data.



Results

The abundant AGN population detected by JWST does not violate constraints on the unresolved X-ray background.



Future Facilities for LyC escape fraction

FORS-Up VLT (December 2026) imaging and low-resolution spectroscopy at 340-1100 nm.

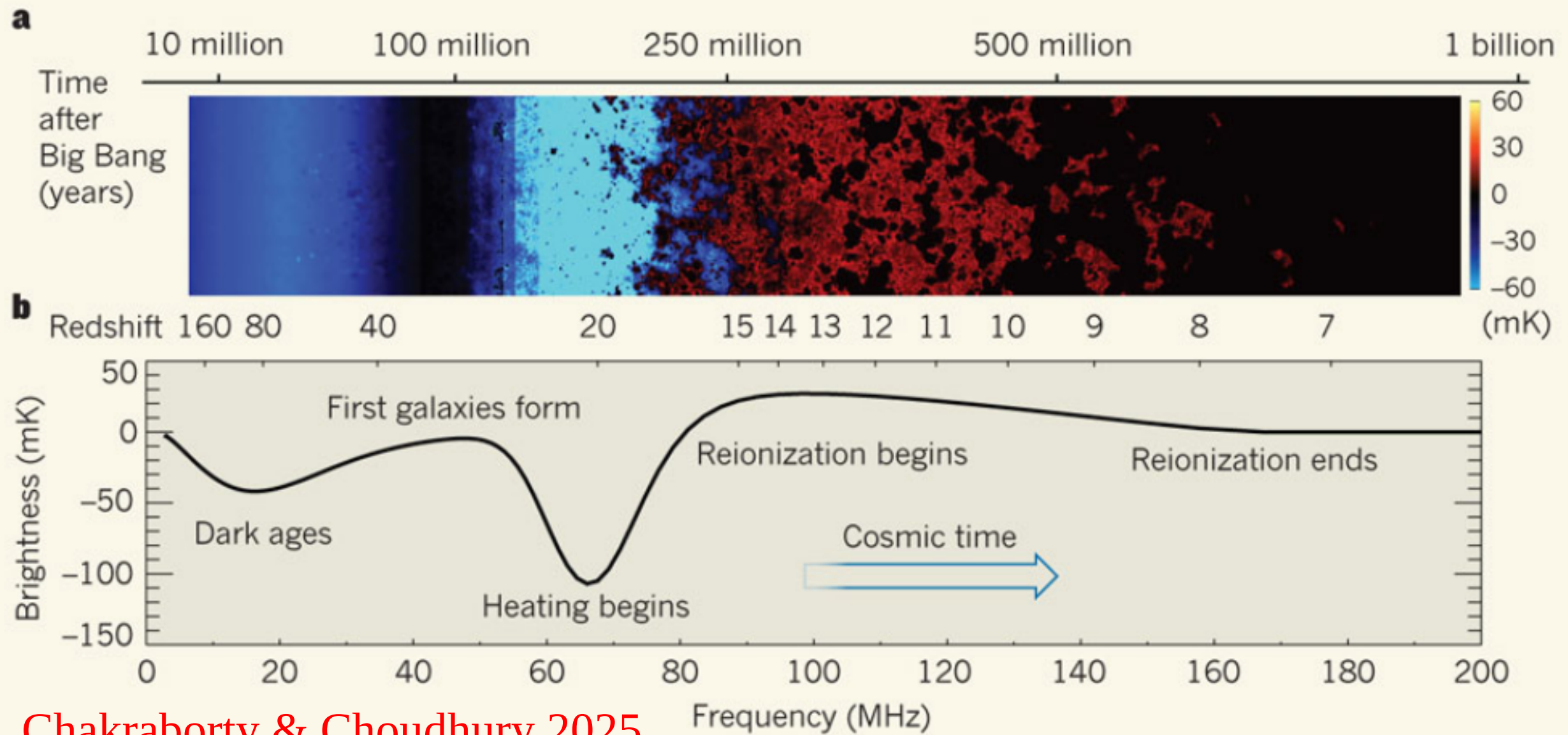
CUBES VLT (December 2029) spectroscopy at 305-400 nm with $R=7000-20000$.

MAVIS VLT (2030) Visible MCAO imager and IFU at 380-935 nm with FWHM=18mas.

BlueMUSE VLT (2031) IFU at 350-580 nm with $R=4000$.

HWO (2040) UV-IR, high spatial resolution imaging and spectroscopy.

SKA



Chakraborty & Choudhury 2025

HI 21cm: tomography of IGM in the Epoch of Reionization and Cosmic Dawn

Summary

1-Direct measurements of large values of the escape fraction ($\sim 75\%$) of LyC photons from bright QSOs ($M_{1450} < -26$) at $z=0-5$.

2-Direct measurements of large values of the escape fraction ($\sim 75\%$) of LyC photons from faint AGNs ($M_{1450} < -18$ at $z \sim 0$ and $M_{1450} < -23$ at $z=4$).

3-Recent results by JWST spectroscopy indicate large space densities of faint AGNs at $z=4-10$. AGN fraction among galaxies is 10-15%.

4-Our fiducial model matches the redshift of Hydrogen and Helium reionization, the integrated Thomson scattering optical depth to Reionization, the constraints on the unresolved XRB.

QSOs/AGNs have not a negligible role on the cosmic hydrogen/helium reionization process.

Thank you
very much!!!

Model assumptions - C

(c) internal absorption at 4 Ryd or a steep ionizing EUV spectrum delay full reionization of HeII until $z=2.8-3.0$, in agreement with observations of the HeII Lyman-alpha forest.

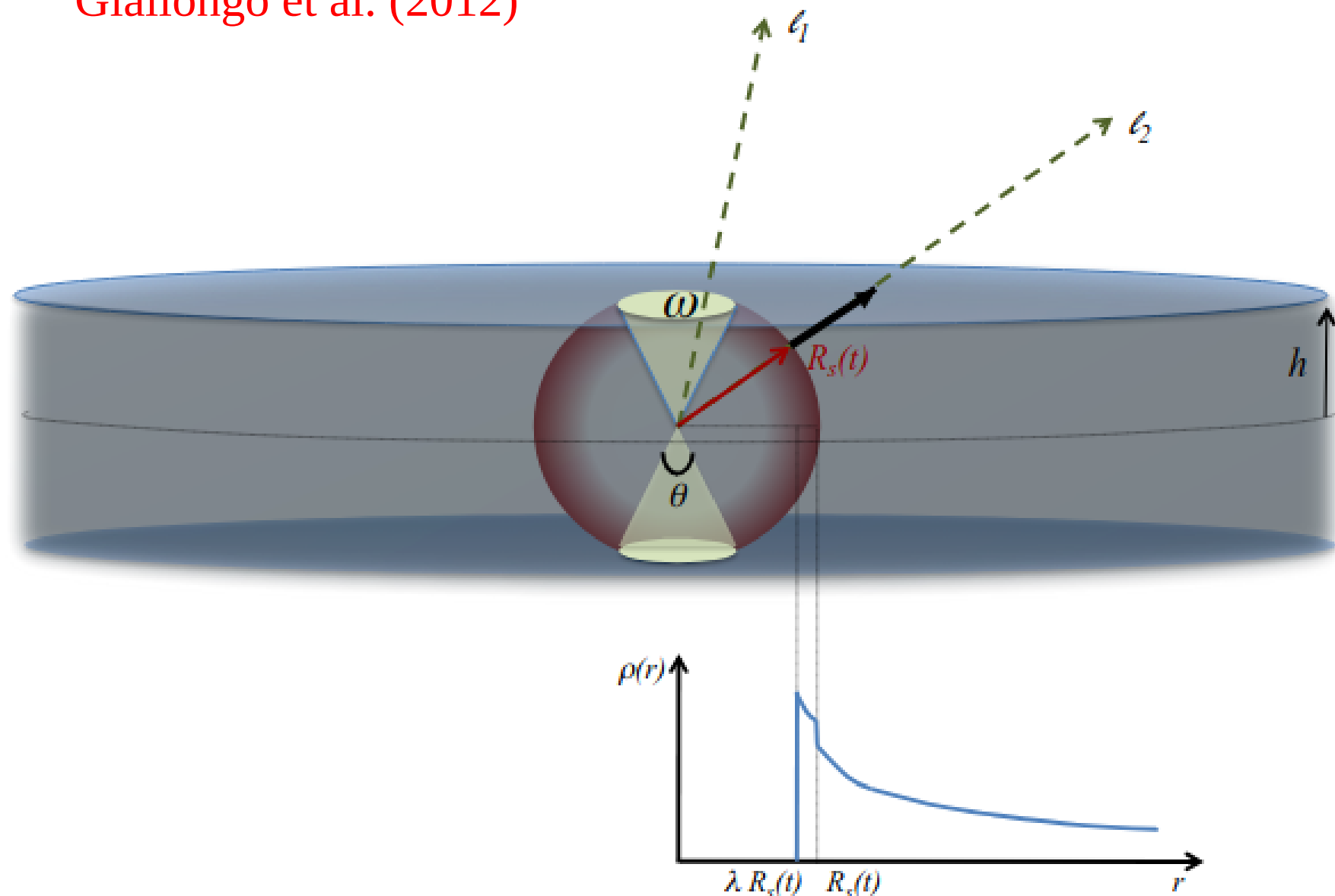
Sub-parsec absorption (between BLR and disk): a close absorber allows a low opacity in HI even if column density is elevated ($\log N_{\text{HI}} > 22-23$), since ionization parameter is $\gg 1$. This is not true for HeII, where absorption is significant.

Even a Compton-thick absorption can have $\tau \leq 1$, assuming a smaller radius. Ionization parameter scales as r^2 .

The "Maiolino Compton thick" hypothesis is critical for reionization by AGN only if the thick absorber is cold, so $T < 10^4$ K and $r \gg 1$ pc, so produced by torus.

Theoretical approach to LyC escape fraction

Giallongo et al. (2012)



A schematic representation of the geometrical effects determining the escape fraction in the blast wave model of AGN feedback.